Article

Meta-Assessment of Metformin Absorption and Disposition Pharmacokinetics in Nine Species

Yoo-Seong Jeong and William J. Jusko *

Department of Pharmaceutical Sciences, School of Pharmacy and Pharmaceutical Sciences, State University of New York at Buffalo, Buffalo, NY 14214, USA; yooseong@buffalo.edu
* Correspondence: wjjusko@buffalo.edu; Tel.: +1-716-645-2855; Fax: +1-716-829-6569

Abstract: The objective of this study was to systematically assess literature datasets and quantitatively analyze metformin PK in plasma and some tissues of nine species. The pharmacokinetic (PK) parameters and profiles of metformin in nine species were collected from the literature. Based on a simple allometric scaling, the systemic clearances (*CL*) of metformin in these species highly correlate with body weight (*BW*) (R^2 = 0.85) and are comparable to renal plasma flow in most species except for rabbit and cat. Reported volumes of distribution (V_{SS}) varied appreciably (0.32 to 10.1 L/kg) among species. Using the physiological and anatomical variables for each species, a minimal physiologically based pharmacokinetic (mPBPK) model consisting of blood and two tissue compartments (Tissues 1 and 2) was used for modeling metformin PK in the nine species. Permeability-limited distribution (low f_{d1} and f_{d2}) and a single tissue-to-plasma partition coefficient (K_p) value for Tissues 1 and 2 were applied in the joint mPBPK fitting. Nonlinear regression analysis for common tissue distribution parameters along with species-specific *CL* values reasonably captured the plasma PK profiles of metformin across most species, except for rat and horse with later time deviations. In separate fittings of the mPBPK model to each species, Tissue 2 was considered as slowly-equilibrating compartment consisting of muscle and skin based on in silico calculations of the mean transit times through tissues. The well-fitted mPBPK model parameters for absorption and disposition PK of metformin for each species were compared with in vitro/in vivo results found in the literature with regard to the physiological details and physicochemical properties of metformin. Bioavailability and absorption rates decreased with the increased *BW* among the species. Tissues such as muscle dominate metformin distribution with low permeability and partitioning while actual tissue concentrations found in rats and mice show likely transporter-mediated uptake in liver, kidney, and gastrointestinal tissues. Metformin has diverse pharmacologic actions, and this assessment revealed allometric relationships in its absorption and renal clearance but considerable variability in actual and modeled tissue distribution probably caused by transporter differences.

Keywords: metformin; pharmacokinetics; absorption; disposition; allometric scaling; minimal physiologically based pharmacokinetic modeling

1. Introduction

Metformin is a biguanide compound that was derived from *Galega officinalis* (French lilac) having an abundant content of the hypoglycemic substance guanidine [1,2]. Although the specific compound metformin was first synthesized in 1920s [3,4] and its use was later replaced by the breakthrough discovery of insulin in the same era [5], experience with guanidine and diguanides for treating diabetes led to development of phenformin [6], buformin [7], and metformin (Glucophage was named by Jean Sterne) in the 1950s [8,9]. However, after phenformin and buformin were withdrawn from the market in most countries due to their high risks of lactic acidosis [10], metformin has been recommended as the first-line oral medication for treatment of type 2 diabetes by the American Diabetes Association (ADA) and the European Association for the Study of Diabetes (EASD) since

2009 [11]. In addition to its antihyperglycemic effect, the United Kingdom Prospective Diabetes Study (UKPDS) reported long-term metabolic effects and reduced cardiovascular risk with metformin [12]. Metformin is increasingly recognized as a potential anticancer agent due to a reduced cancer incidence in diabetic patients treated with the drug [13–15], and recently, patients taking metformin were associated with a reduced risk of COVID-19-related mortality [16,17]. The history of metformin from its discovery in the 18th century to clinical uses for over 60 years is well-summarized in the literature [18], and the drug is now widely used with more than 500 million prescriptions in United States with growth trends since 2000 [19].

Although its mechanism of action remains unclear even with the long-term experiences of clinical use, the blood glucose-lowering effect of metformin is attributed to several tissues. The major mode of its pharmacological action is decreased hepatic gluconeogenesis by modulation of mitochondrial enzymes and by the antagonistic regulation of the glucagon signaling pathway [20,21]. In vitro studies in rodents showed that metformin improved insulin sensitivity of muscle by increasing the expression and activity of insulin receptors, leading to increased insulin-dependent glucose uptake in cells [22–24]. In addition, increased glucose uptake into the intestinal mucosa [25] and reduced intestinal glucose absorption [26] were observed in metformin-treated rats. A compartmental model accounting for amounts of metformin in plasma, liver, muscle, and gastrointestinal (GI) tract provided an insightful quantitative assessment of glucose-lowering effects that differ with route of administration in diabetic rats [27]. An alternative model for glucose production inhibited by metformin distributed to a biophase compartment described its blood-glucose lowering effect in diabetic rats at different doses [28]. Pharmacodynamic studies of metformin in rat or man describing its effects over a range of doses are few.

Oral absorption of metformin from the immediate-release dosage forms is incomplete in man, with an estimated population mean of 55% for bioavailability [29]. Metformin, a strong base with pKa = 11.8 [30], is present mostly as a cationic form at biologically relevant pH ranges and has a high water solubility larger than 100 mg/mL [31]. Its hydrophilicity (log P = −1.43) [32] is associated with the low intestinal [33] and cell membrane permeability [34], which is recognized as a primary limiting step for metformin oral absorption and accounts for its insignificant metabolism in the liver. Metformin is mainly eliminated by renal excretion mediated by transporters, including organic cation transporters (OCT1 and OCT2) and multidrug and toxin extrusion proteins (MATE1 and MATE2) [35]. Dosage adjustments are thus necessary for patients with severe renal dysfunction [36–38]. In healthy subjects, a longer half-life of metformin in erythrocytes (23.4 h) was observed compared to plasma (2.7 h) [39], but this may be attributed to the time frames assessed. Similarly, a longer half-life of metformin was also observed in following urinary excretion rates (9.3 to 19.0 h) [37,40]. Metformin concentrations in tissues have been measured using radiolabeled compounds (i.e., ^{14}C-label for mouse and ^{11}C-label for man), as well as use of PET (Positron Emission Tomography) scanning [41,42]. However, a limited number of time points/tissues, potential involvement of its metabolite(s), and indistinguishability of intra- and extracellular and the intravascular fractions using PET are limiting factors. The drug exhibits either poly-exponential or power function disposition with uncertainties regarding its distribution kinetics, the terminal half-life, and recoveries in urine.

When only pharmacokinetic (PK) profiles in plasma are available, minimal physiologically based pharmacokinetic (mPBPK) models allow a rational interpretation of plasma and expected tissue PK by the incorporation of physiological and anatomical elements into PK analyses [43]. In line with this, allometric scaling is often utilized to relate drug disposition processes to body size [44]. The renal clearance of metformin was reported to have a simple allometric relationship with body weight (*BW*) with a common exponent of 0.75 [45]. However, traditional allometric scaling assessing PK parameters in relation to *BW* (i.e., $Y = a \cdot BW^b$) among species is considered empirical [46]. Thus, integrating allometric features into mPBPK modeling is useful for interspecies scaling of PK characteristics. Previously, mPBPK models were successfully applied for across-species fitting and

scaling of full PK profiles of moxifloxacin [43], dexamethasone [47], and several monoclonal antibodies [48]. Despite abundant PK data for metformin in various species from its wide use in clinical/veterinary and experimental settings for over 60 years, there has been only limited quantitative analysis assessing interspecies relationships regarding PK properties of metformin [49,50].

In reviewing the extensive literature on metformin PK, we first assessed its clearance (CL) in relation to BW and renal plasma flow (RPF) across species using traditional allometry. We then employed mPBPK models to quantitatively analyze metformin PK in all nine species. Joint fittings using mPBPK models that adopted the physiological and anatomical properties of each species were applied to obtain common PK parameters with conserved features across the species seeking a minimal number of parameters that could describe all data. As a third step, a mPBPK model structure based on in silico-predicted tissue constituents was used to further determine and compare the species-dependent PK parameters related to absorption and disposition of metformin for each of the nine species. This systematic review of literature datasets and quantitative analyses of metformin PK in plasma and some tissues of all available species should be useful for further evaluation of the pleiotropic pharmacological effects of metformin.

2. Results

2.1. Allometric Scaling

The PK parameters of metformin after the intravenous (IV) and oral doses found in nine species are summarized in Table 1. The raw data for metformin PK in dog were provided by Johnston et al. [51], and all others were digitized for the current analysis. When PK parameters in any species were found to be variable among multiple studies (e.g., CL values ranging from 12.7 to 81.7 mL/min/kg in mouse and from 6.0 to 42.8 mL/min/kg in rat; Supplementary Table S1), PK data were selected on the basis of the richness of sampling time points, duration of sampling periods, details of study design, and alignment of CL values with basic allometric scaling. It is noted that, due to variable PK profiles depending on the oral doses in rats in previous literature that included the same IV doses (50, 100, and 200 mg/kg) [52], another oral PK profile at a similar experimental setting [53] was considered for the individualized analysis.

Table 1. Literature reports and pharmacokinetic parameters of metformin after intravenous and oral doses in various species.

Reference	Species	Strain	Sex	Body Weight (kg)	Dosing Route	Dose (mg/kg)	Assay	CL (mL/min/kg)	CL/F (mL/min/kg)	CL_R (mL/min/kg)	RPF (mL/min/kg)	V_{SS} (mL/kg)
Higgins et al. (2012) [54]	Mouse	FVB	M	-	IV *	5	LC-MS/MS	81.7		40.0	60 [a]	1840
					PO *	10	LC-MS/MS		138			
Nakamichi et al. (2013) [55]	Mouse	C57BL/6J	M	-	IV Infusion	0.12 mg/kg/min	HPLC-UV	60.7		60.3		
					PO *	50, 175	HPLC-UV		77.5, 59.8 **			
Choi et al. (2006) [52]	Rat	Sprague-Dawley	M	0.20–0.31	IV *	50, 100, 200	HPLC-UV	23.6–26.4		17.8–19.5	24.8 [b]	586–693
					PO	50, 100, 200	HPLC-UV		76.0–82.0	37.4–39.6		
Choi et al. (2010) [53]	Rat	Sprague-Dawley	M	0.19–0.30	IV	100	HPLC-UV	14.7		11.6		383
					PO *	100	HPLC-UV		34.1	30.9		
Bouriche et al. (2020) [56]	Rabbit	New Zealand	F	-	IV *	5	HPLC-UV	2.05			13.1 [c]	321
					PO *	5	HPLC-UV		5.67			
Choi and Choi (2003) [57]	Rabbit	New Zealand	M	2.0–2.2	PO *	15	HPLC-UV		6.01			
Michels et al. (1999) [58]	Cat	Domestic shorthair	-	4.3–6.5	IV *	25	HPLC-UV	2.5		2.17	13.8 [d]	550
					PO *	25	HPLC-UV		5.21			
Nelson et al. (2004) [59]	Cat	-	M	4–5	PO *	50 mg	HPLC-UV		9.05			
Shen et al. (2016) [60]	Monkey	Cynomolgus	M	5–7	IV *	3.9	LC-MS/MS	11.2		10.7	9.61 [e]	802 **
Heinig and Bucheli (2004) [61]	Monkey	Cynomolgus	-	-	PO *	250	LC-MS/MS		93.5 **			
Patel et al. (2017) [62]	Minipig	Hanford	M	14.3	IV *	0.5	LC-MS/MS	9.7			9.36 [f]	2260 **
					PO *	5	LC-MS/MS		14.8 **			
Johnston et al. (2017) [51]	Dog	Mixed	-	25.7–29.2	IV *	24.8	FIA-MS/MS	24.1			17.9 [g]	10100
					PO *	19.1	FIA-MS/MS		77.7			

Table 1. *Cont.*

Reference	Species	Strain	Sex	Body Weight (kg)	Dosing Route	Dose (mg/kg)	Assay	*CL* (mL/min/kg)	*CL/F* (mL/min/kg)	*CL$_R$* (mL/min/kg)	*RPF* (mL/min/kg)	*V$_{SS}$* (mL/kg)
Sirtori et al. (1978) [36]	Man	Healthy	4 M 1 F	64–81	IV *	926 mg	GC-MS	6.13		4.65	7.81 [b]	432 **
Pentikäinen et al. (1979) [40]	Man	Healthy	1 M 2 F	58–63	IV *	500 mg	LSC	7.61		7.52		856 **
			2 M 3 F	56–80	PO *	500 mg	LSC		16.3	7.06		
Tucker et al. (1981) [37]	Man	Healthy	4 M	64–83	IV *	250 mg	GC-EC	10.1		7.83		511 **
					PO *	500, 1500 mg	GC-EC		18.9, 21.5	7.42, 7.16		
Lee and Kwon (2004) [63]	Man	Healthy	22 M	55–89	PO *	500 mg	HPLC-UV		16.2			
Hustace et al. (2009) [64]	Horse	-	-	531.8	IV *	6 g	HPLC-UV	10.8			12.1 [h]	2250 **
					PO *	6 g	HPLC-UV		152			

* Dataset included in the modeling analysis. ** Calculated from the digitized data. [a] Thuesen et al. (2014) [65]. [b] Brown et al. (1997) [66]. [c] Sweeny et al. (2009) [67]. [d] Lindstedt and Schaeffer (2002) [68]. [e] Values adopted in Simcyp V19 [69]. [f] Suenderhauf and Parrott (2013) [70]. [g] Wesolowski et al. (2019) [71]. [h] Holdstock et al. (1998) [72].

As shown in Figure 1, the reported *CL* values for metformin showed a simple allometric relationship with *BW* of the nine species (R^2 = 0.85). Despite this reasonable correlation, the systemic *CL* values of metformin in rabbit and cat deviate from the fitted relationship (with a factor of 6.33 and 4.49). Except for these two species, *CL* values were comparable with *RPF*, indicating a high extraction ratio of metformin in the kidney, and were consistent with evidence that metformin is mainly eliminated via renal excretion [40,73].
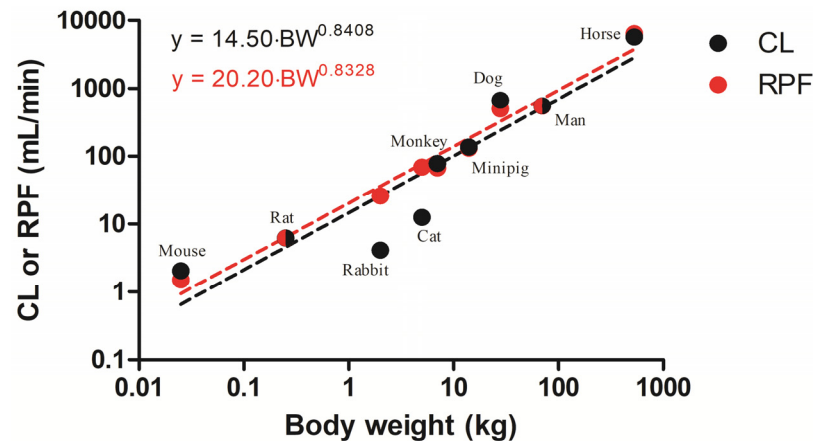
Figure 1. Allometric relationships between literature-reported metformin *CL* (black) and renal plasma flow (*RPF*) values (red) and body weights of 9 species (Table 3, see below). Except for rabbit and cat, the systemic clearance of metformin was comparable to *RPF*. Lines were fitted to the indicated allometric relationships ($y = a \cdot BW^b$, where *BW* is the body weight).

2.2. Joint Fittings of IV Profiles

The metformin PK data were first jointly analyzed using the common parameters across the species adopted in the mPBPK model (K_p, $f_{d,total}$, f_{d1}, f_{d2}, and f_t), along with the individual optimized *CL* for each species. Figure 2 shows the mPBPK model structure used for metformin PK and the differential equations for the current analysis are described in Methods section. As shown in Figure 3, the plasma concentrations across species ranged from about 1000 to 0.001 µg/mL, with rapid and slower phases often extending to 72 h. A wide range of IV doses were given (Table 1), and the plasma concentrations were not normalized for the dose. The mPBPK model anticipates triexponential disposition profiles that appear in all species. Consistent with its hydrophilicity (log P = −1.43) [32] and low passive permeability [74], the assumption of perfusion-limited distribution (i.e., $f_{d1} + f_{d2} = 1$) did not adequately capture the PK data in our preliminary mPBPK modeling. Thus, it was reasoned that the sum of the two fractional distribution parameters would be less than 1 and conserved across the species in the joint fitting approach (Equation (7)). In addition, a consideration of different K_p values for each tissue compartment (K_{p1} and K_{p2}) did not work well, leading to unreliable estimates (extremely high CV%) for parameters K_{p1}, K_{p2}, and f_t. As a result, the PK profiles were reasonably captured by the current mPBPK model, except for rat and horse, with later time deviations. However, the late PK data in horses were difficult to digitize and the mouse data lacked a terminal phase. The three IV dose profiles for man came from three different studies (Table 1) and all were very well-captured. Despite these divergent fittings, CV% values for the distribution parameters of the joint mPBPK model were all less than 10% (Table 2). The fitted *CL* for each species from the joint fitting are listed in Table 3 (all CV% less than 15%). Based on the single K_p assumption, the physical volume of Tissue 1 ($0.16 \cdot BW$) was smaller than Tissue 2 ($0.77 \cdot BW$). The $f_{d,total}$ is 0.0457, which implies that 4.57% of the drug is subjected to extraction from the blood during each passage through tissues, as the total distributional clearance CL_D is $Q_{CO} \cdot f_{d,total}$ (Equation (2)). The distributional clearance to Tissue 1 or 2 can be calculated by multiplying either f_{d1} or f_{d2} by the cardiac output (Q_{CO}) of each species, indicating that Tissue 1, which has a shorter *MTT*, is more rapidly equilibrated

than Tissue 2 ($MTT_1 = V_1 K_p / (Q_{CO} f_{d1} R_b)$ and $MTT_2 = V_2 K_p / (Q_{CO} f_{d2} R_b)$). The overall K_p value is 1.29, which is midrange to many V_{SS} values found by noncompartmental analysis (NCA) (0.321 to 2.26 L/kg, except for dogs), as listed in Table 1. The V_{SS} value for dogs calculated by NCA using the averaged concentration–time data was 10.1 L/kg, which was accompanied by the underestimation of the systemic CL for dogs in the joint fitting (9.01 mL/min/kg, compared to the reported CL of 24.1 mL/min/kg) within a restricted range of distribution parameters. Due to the model prediction showing the terminal phase with a longer half-life than the limited observations in mouse (Figure 3), divergent NCA and jointly fitted CL values were observed (Table 3).

Table 2. Pharmacokinetic parameters of metformin jointly fitted to the minimal physiologically based pharmacokinetic model across 9 species [a,b].

	Definition	Estimate (CV%)
K_p	Tissue-to-plasma partition coefficient	1.29 (9.67)
$f_{d,total}$	Total sum of fractional distribution parameters ($f_{d1} + f_{d2}$)	0.0457 (8.12)
f_{d1}	Fractional distribution parameter for Tissue 1	0.0390 (8.91)
f_{d2}	Fractional distribution parameter for Tissue 2	0.00677 (7.59) [c]
f_t	Fraction of total tissue volume for Tissue 1	0.172 (8.87)

[a] The jointly-fitted CL values are listed in Table 3. [b] AIC = 248.19. [c] Estimated as a secondary parameter by $f_{d2} = f_{d,total} - f_{d1}$.

Table 3. Comparison of systemic clearance values of metformin for 9 species based on the indicated methods of calculation/estimation (CV% obtained by fitting).

Species (Body Weight, kg)	Reported CL (mL/min/kg) *	NCA CL (mL/min/kg)	mPBPK Joint CL (mL/min/kg)	mPBPK Individual CL (mL/min/kg)	RPF (mL/min/kg)
Mouse (0.025)	81.7	81.8	32.9 (6.05)	65.8 (26.9)	60
Rat (0.25)	23.6–26.4	20.8–21.3	23.5 (3.80)	23.2 (4.00)	24.8
Rabbit (2)	2.05	2.05	1.43 (14.5)	1.30 (38.2)	13.1
Cat (5)	2.5	2.55	2.90 (4.78)	2.78 (7.11)	13.8
Monkey (7)	11.2	11.0	12.5 (5.87)	15.1 (7.71)	9.61
Minipig (14)	9.7	9.18	6.08 (6.37)	9.32 (9.72)	9.36
Dog (28)	24.1	20.2	9.01 (4.15)	19.3 (15.8)	17.9
Man (70)	6.13–10.1	6.19–9.47	5.20 (3.77)	7.74 (4.19)	7.81
Horse (530)	10.8	8.25	5.51 (5.49)	6.89 (11.0)	12.1

* References are provided in Table 1.
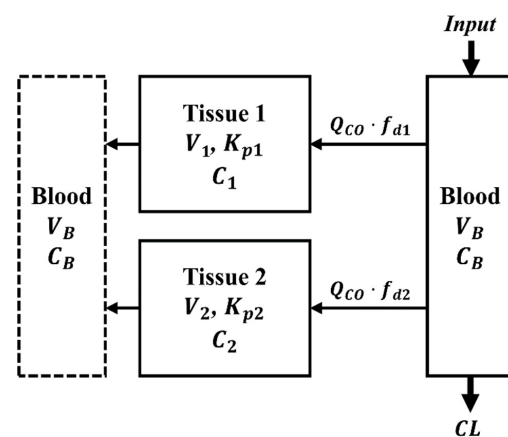
Figure 2. The minimal physiologically based pharmacokinetic model with two tissue compartments. A single K_p value ($K_{p1} = K_{p2}$) was used in the joint fitting, while the cardiac output (Q_{CO}) was divided into tissue blood flow to each compartment ($Q_1 + Q_2 = Q_{CO}$) in the separate fittings. Symbols are defined in the text and in Table 2 and Table 5 (see below).
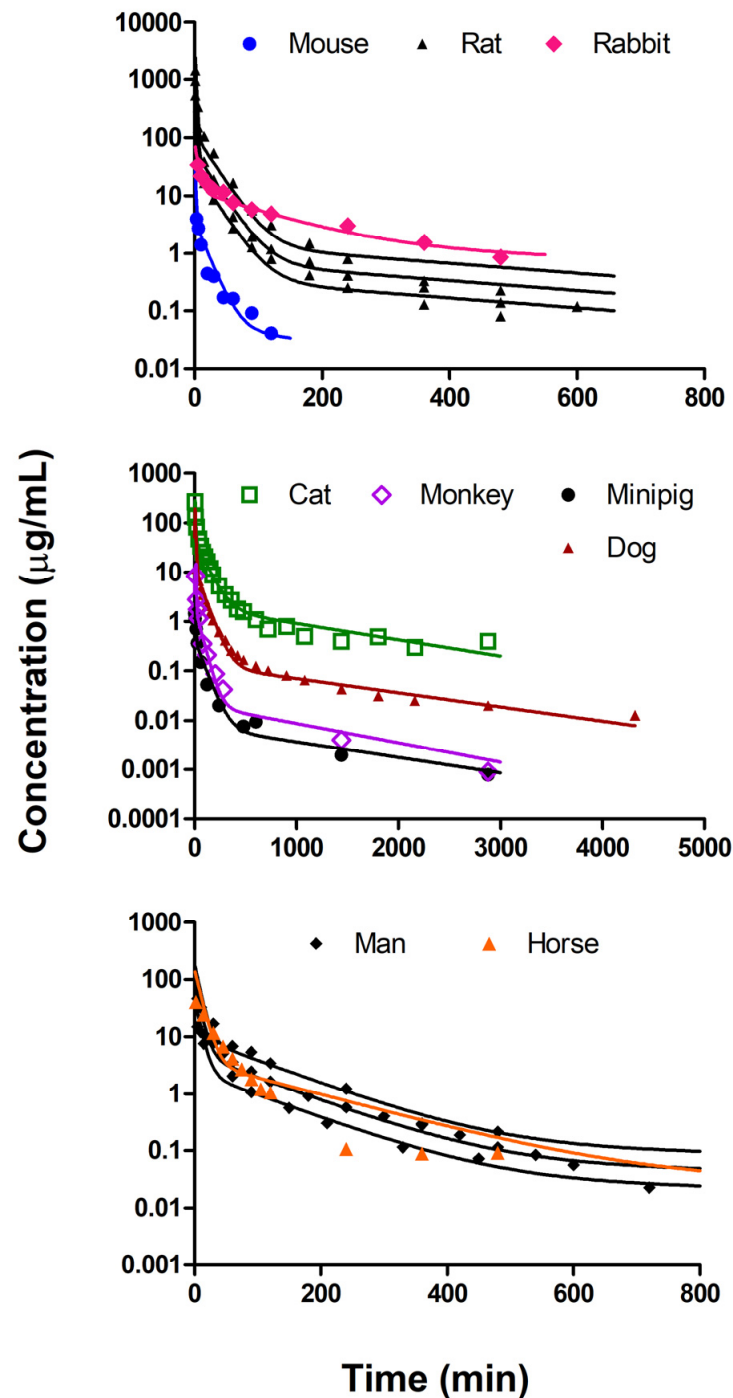
Figure 3. Simultaneous fitting of metformin pharmacokinetics dosed intravenously in 9 species to the minimal physiologically based pharmacokinetic model in Figure 2. Fitted profiles are in separate panels for visual clarification for the indicated species. The doses and fitted parameters are listed in Tables 1 and 2. The three curves for man are for different doses from three studies.

2.3. Individual Oral and IV Fittings

In order to investigate potential differences in PK variables for metformin across the species, we carried out further model fittings of both IV and oral PK profiles separately for each of the nine species. Having multiple PK profiles in each species adds greater certainty in resolving model parameters. As shown in Figure 4, all PK profiles were well-captured. Tissue lumping theories [75–78] state that the major organ(s) composing the rapidly and slowly equilibrating compartments (Tissues 1 and 2) that, in turn, govern the exponential

components/shapes of the systemic PK may not be identifiable without information on tissue PK. However, muscle was included in Tissue 2, since the f_t estimate of 0.172 from the joint fitting (Table 2) was small. Using S_{eff} values in a WB-PBPK structure for rats [79], the tissue permeability coefficient P was estimated to be 0.0102×10^{-6} cm/s with a CV% of 29.4% ($R^2 = 0.98$). As a result, in silico calculations (Table 5) consistently indicate that skin may be the kinetically largest tissue with the longest MTT for a variable range of permeability coefficients. A rule of thumb for lumping kinetically large tissues suggests that tissues within a two-fold difference in MTT may be lumped into a single compartment [75], which was satisfied by MTT values calculated from the in vitro PAMPA P for muscle and skin (Table 5). The brain, the second-largest tissue based on the case of fitted P that satisfies the acceptance condition with a factor of 1.62, was not included in Tissue 2, considering the variable K_p values for rat brains (cf. in vivo K_p ranged from 0.2 to 1.48 (Table 6, see below)), compared to an in silico value of 0.86 (Table 5), where the involvement of the efflux transport of metformin by P-glycoprotein [80] may reduce K_p and, thus, MTT. Based on these considerations, the mPBPK model in our separate fitting approach utilizes the blood flow rate and anatomical volume of skin and muscle to define Tissue 2, with the fractional tissue volume ($f_t = V_2/(BW - V_B)$) ranging from 0.472 to 0.678 and blood flow (Q_2/Q_{CO}) from 0.217 to 0.563 (Supplementary Table S2).
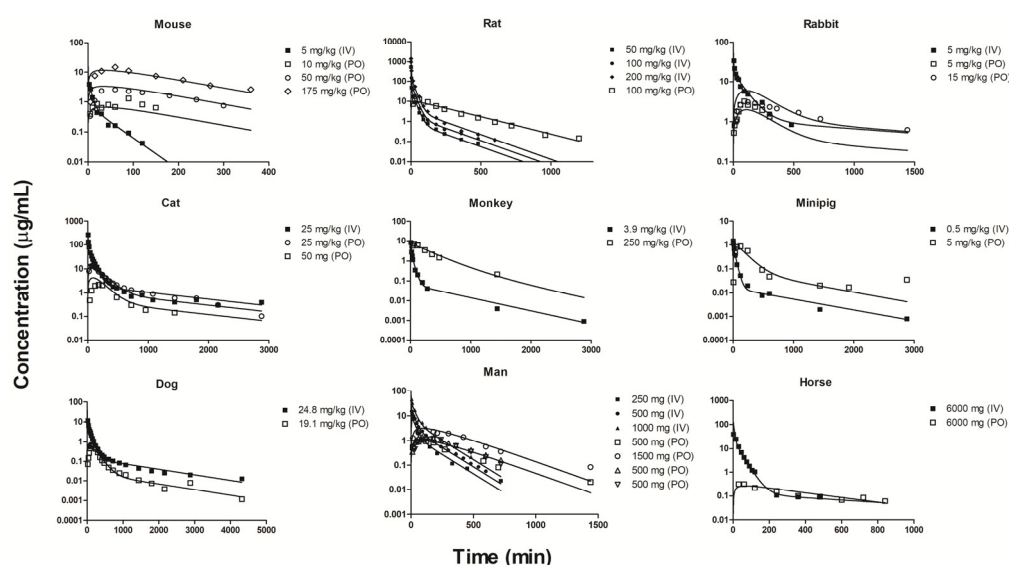
Figure 4. Fitting of intravenous and oral pharmacokinetics of metformin individually for 9 species to the mPBPK model. The slowly-equilibrating compartment (Tissue 2) was assumed to consist of skin and muscle (i.e., $Q_2 = Q_{SK} + Q_{MU}$, $V_2 = V_{SK} + V_{MU}$). Fitted parameters are listed in Table 4.

The IV and oral PK profiles were reasonably captured (Figure 4) in all species with the fitted parameters listed in Table 4. It is noted that the 48-h time point in the oral PK profile in minipig was excluded in the current analysis as an obvious outlier as inclusion produced parameter estimates with an unreliable CV% and an extremely shallow terminal phase. It should be noted that the terminal phase slope in flip-flop kinetics is dependent on the total escaping rate from the absorption site (k_a), not $F \cdot k_a$. The half-lives of k_a in mouse, rat, and man are 1.85, 2.82, and 1.74 h (Table 4), which are longer than model-predicted terminal phase half-lives, leading to flip-flop kinetics in these species (Figure 4). As shown in Table 4, the f_{d1} values were smaller than f_{d2} for each species, while K_{p1} was smaller than K_{p2} except for rat, indicating that MTT_2 is longer than MTT_1. Except for f_{d1} for mouse and K_{p2} for horse, the largest CV% of the primary estimates was 93.5%, but the others were quite small (Table 4), indicating reasonable model performances.

Table 4. Pharmacokinetic parameters of metformin separately fitted to the minimal physiologically based pharmacokinetic model across 9 species.

	Estimate (CV%)								
	Mouse	**Rat**	**Rabbit**	**Cat**	**Monkey**	**Minipig**	**Dog**	**Man**	**Horse**
K_{p1}	0.921 (81.0)	0.575 (10.2)	0.479 (19.9)	0.405 (20.6)	0.615 (21.2)	0.875 (20.5)	4.31 (38.1)	0.484 (13.3)	0.175 (27.4)
K_{p2}	1.44 (50.0)	0.466 (9.62)	2.15 (93.5)	2.69 (18.6)	3.27 (17.5)	4.13 (20.8)	7.53 (30.2)	0.669 (11.9)	0.884 (213)
f_{d1}	0.379 (163)	0.0694 (14.5)	0.106 (36.2)	0.0789 (38.5)	0.158 (32.3)	0.966 (34.9)	0.765 (83.6)	0.993 (44.4)	0.106 (46.3)
f_{d2}	0.239 (69.5)	0.0157 (11.7)	0.0184 (29.0)	0.0321 (14.3)	0.0482 (21.9)	0.0472 (22.7)	0.130 (30.8)	0.171 (22.3)	0.0455 (81.1)
CL (mL/min) [a]	1.65 (26.9)	5.81 (4.00)	2.60 (38.2)	13.9 (7.11)	106 (7.71)	131 (9.72)	540 (15.8)	542 (4.19)	3650 (11.0)
F	0.995 (27.5)	0.675 (7.28)	0.334 (11.0)	0.501 (8.63)	0.157 (10.3)	0.474 (13.6)	0.203 (17.2)	0.485 (5.54)	0.0873 (11.7)
k_a (h^{-1})	0.375 (15.4)	0.246 (4.05)	0.424 (16.0)	0.402 (11.1)	0.209 (9.71)	0.390 (15.7)	0.390 (13.0)	0.253 (5.42)	0.144 (11.7)
V_{SS} (L/kg) [b]	1.21 (51.5)	0.536 (7.48)	1.49 (79.8)	1.56 (16.9)	1.89 (16.3)	2.65 (18.8)	6.00 (30.5)	0.603 (7.36)	0.574 (156)

[a] Fitted CL values are listed in Table 3. [b] V_{SS} calculated as a secondary parameter ($V_{SS} = (V_B + V_1 \cdot K_{p1} + V_2 \cdot K_{p2})/BW$).

Table 5. A priori in silico calculation of the tissue distribution parameters (K_p and f_d) for 11 typical tissues of rats in the WB-PBPK. The K_p values were predicted using the Poulin and Theil [81] and Berezhkovskiy [82] methods built in the GastroPlus PBPK simulator, except for the gut. In vitro PAMPA P (0.5×10^{-6} cm/s) and fitted P (0.0102×10^{-6} cm/s) were used to calculate the mean transit time (*MTT*).

| Tissue [a]	K_p	In Vitro PAMPA P		Tissue [a]	K_p	Fitted P to In Vivo Profile	
		$f_{d,tissue}$	*MTT* (min)			$f_{d,tissue}$	*MTT* (min)
Kidney	0.82	0.88	0.176	Kidney	0.82	0.0423	3.66
Lung	0.83	0.0648	0.199	Heart	0.82	0.00137	7.54
Heart	0.82	0.832	0.324	Gut [b]	0.81	0.0357	8.53
Liver	0.76	0.86	0.391	Liver	0.76	0.0393	8.56
Adipose	0.16	0.959	0.589	Adipose	0.16	0.0632	8.94
Gut [b]	0.81	0.975	0.636	Lung	0.83	0.0727	9.42
Spleen	0.81	0.588	0.893	Muscle	0.79	0.0179	25.1
Bone [c]	0.47	0.744	1.23	Spleen	0.81	0.0274	29.3
Brain	0.86	0.425	2.24	Bone [c]	0.47	0.0113	33.3
Muscle	0.79	1	4.84	Brain	0.86	0.1930	84.6
Skin	0.69	0.913	7.30	Skin	0.69	0.0486	137

[a] Tissues were arranged in ascending order of *MTT* for each case. [b] K_p value predicted by Method 1 in Simcyp V19 (Berezhkovskiy [82]).; [c] K_p value for red marrow predicted by GastroPlus 9.8.

The estimated PK parameters related to oral absorption of metformin from the separate fittings are shown in Figure 5. The model-fitted bioavailability F for the nine species showed a decreasing trend with increasing *BW*. While the k_a values were statistically independent of *BW* (i.e., allometric exponent with statistically insignificant difference from 0), the effective absorption rate constant ($F \cdot k_a$) was highly correlated with *BW* with an allometric exponent of 0.257 (R^2 = 0.54). This is consistent with a common allometric exponent of 0.25 found for the rate constants [44]. According to the Biopharmaceutics Classification System (BCS) [83], metformin is considered a Class III drug based on its high water solubility as a hydrochloride salt (i.e., >100 mg/mL) [31] and low intestinal effective permeability (e.g., $P_{eff,rat}$ = 0.27×10^{-4} cm/s) [33]. Based on the assumption of instantaneous solubilization of metformin into the fluid volumes of the stomach and small intestine (V_{Lumen} values summarized in Supplementary Table S2), $Dose/V_{Lumen}$ was estimated to be far below 100 mg/mL for the maximum dose of 175 mg/kg in mouse (i.e., 10.9 mg/mL). Therefore, expecting that intestinal permeability is the major determinant governing metformin absorption, the effective permeability (P_{eff}) was estimated by considering the GI tract as a cylinder (i.e., $F \cdot k_a = \frac{2P_{eff}}{R}$, where R is the gut radius). These were particularly higher in minipig, man, and dog than other species.

2.4. Tissue Distribution of Metformin

Part of this literature review included the assessment of actual tissue-to-plasma partition coefficients of metformin. All available measurements are listed in Supplementary Table S3, with means and ranges summarized in Table 6. In vivo data could be mostly found for rats and mice, except for protein binding and erythrocyte distribution. The drug appeared to sequester most highly in the GI tract, kidney, and liver, with tissue-to-plasma ratios of 3 or greater. Large values are expected in kidney owing to the robust transport mechanism and probable inclusion of tubular fluid with excreted drug in the measurements. The high ratios in the liver and kidney were not anticipated when using the tissue K_p prediction methods (Table 5) for metformin in rats, as these methods do not account for the role of transporters. Muscle is the dominant tissue in the body by weight and has low tissue-to-plasma ratios of 0.6 to 1.0 that are in accordance with the predicted value (0.79). This likely explains the overall low K_p and V_{SS} values found when fitting mouse and rat data using the mPBPK model (Table 4). Using the in vivo tissue K_p values listed in Table 6, along with the muscle K_p assumed to be the same for the unavailable tissues, the calculated V_{SS} ($V_{SS} = V_B + \sum V_{T,i}K_{p,i}$) [84] was 2140 mL/kg for mouse and 777 mL/kg for

rat (Supplementary Table S4), comparable to the observed V_{SS} of 1840 mL/kg for mouse and 586–693 mL/kg for rat (Table 1).
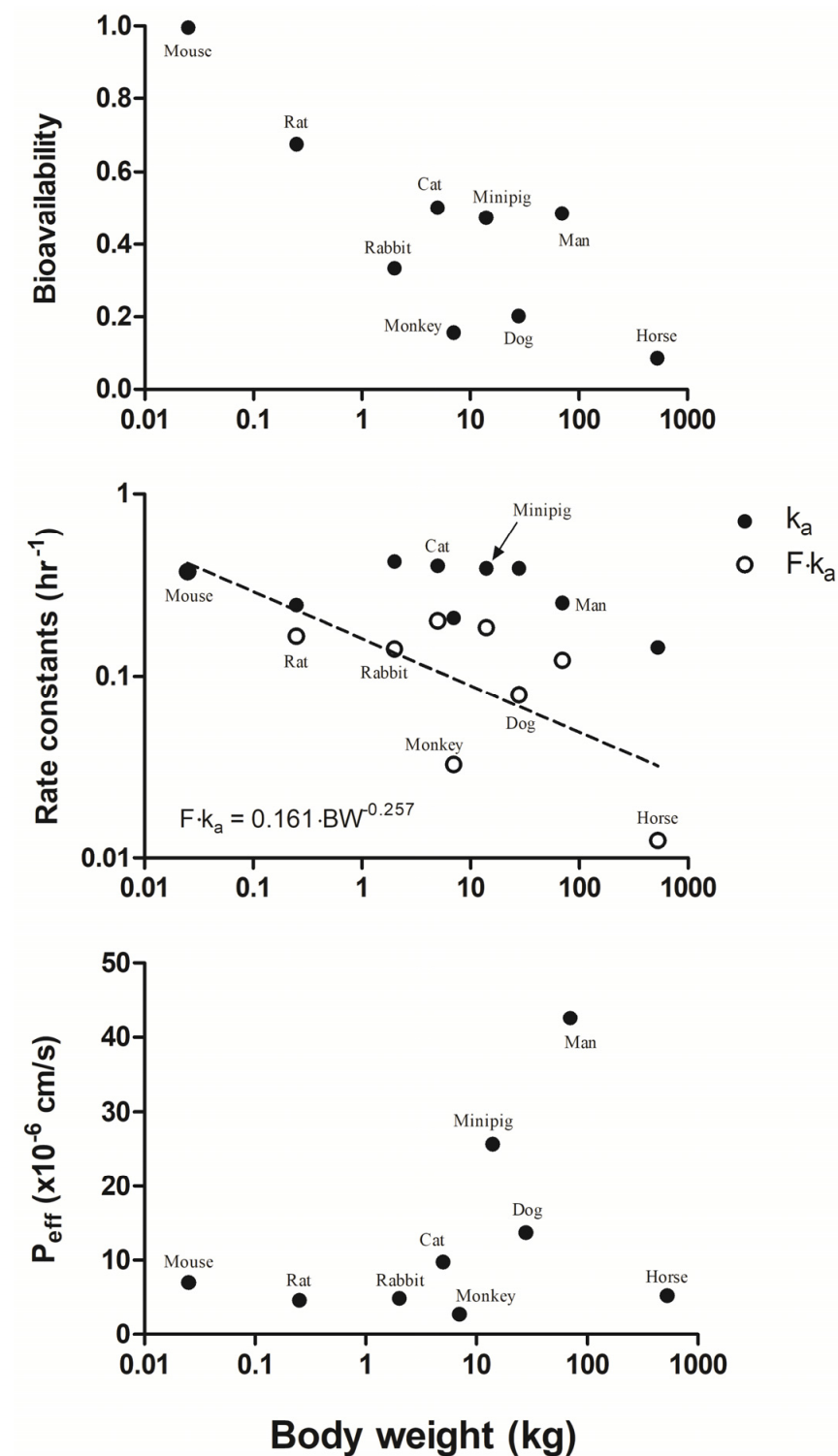
Figure 5. Fitted pharmacokinetic parameters related to oral absorption of metformin in relation to body weights, including bioavailability (F), absorption rate constants (k_a and $F \cdot k_a$), and intestinal effective permeability (P_{eff}). The fitted parameters for each species are listed in Table 4.

Table 6. Summary of measured tissue and blood partition coefficients in four species *.

Species	Tissue	.	Mean (Range) **
		No. of values	K_p
Mouse	Liver	16	3.47 (1.72–7.10)
	Brain	5	0.213 (0.0354–0.257)
	Kidney	12	8.74 (3.35–20.5)
	Muscle	8	1.03 (0.359–2.06)
	Heart	3	0.610 (0.519–0.712)
	Adipose	1	0.471
	Stomach	4	6.38 (4.67–9.03)
	Small intestine	6	11.3 (0.837–21.1)
	Colon	4	7.72 (4.52–13.9)
	Salivary gland	2	3.03 (2.60–3.45)
Rat	Liver	10	3.07 (0.368–6.83)
	Brain	5	0.8 (0.2–1.48)
	Kidney	9	4.04 (0.128–5.92)
	Muscle	2	0.597 (0.455–0.738)
	Spleen	1	0.956
	Gut	1	4.63
		No. of values	R_b
Rat	Blood	2	1.18 (0.98–1.37)
Man	Blood	2	1.03 (0.83–1.23)
	(free fraction in the)	No. of values	f_u
Rat	Plasma	3	0.873 (0.849–0.897)
Dog	Plasma	3	0.904 (0.83–0.951)
	Blood	1	0.920
Man	Plasma	6	0.938 (0.75–1.0)
	Blood	1	0.932

* Detailed literature information is listed in Supplementary Table S3. Data from normal (nondiabetic) species were included after an outlier test based on the interquartile range rule. ** For data presented as a range from a single study, the average value of the maximum and minimum was adopted.

3. Discussion

Metformin is widely used as a first-line agent for the treatment of type 2 diabetes. Its antihyperglycemic effect is mainly achieved by decreasing hepatic gluconeogenesis and glycogenolysis and by increasing the insulin sensitivity of muscle tissue [85,86]. Its advantages include insignificant risks of clinical hypoglycemia, which is a serious side effect caused by antidiabetic agents such as insulin and sulfonylureas [87]. In addition, metformin reduces plasma triglycerides and low-density lipoproteins (LDL) [88–91], which may decrease the risk of cardiovascular disease. The drug has received considerable attention due to a reduced cancer incidence in diabetic patients treated with metformin [13–15]. Inhibition of mitochondrial complex I activity has been proposed to be the mechanism of the antitumor effect [92,93] that could be mostly observed at supra-pharmacological concentrations of metformin (i.e., *IC*50 of 19–66 mM) [94,95], while the blood glucose lowering effect was mediated by increased mitochondrial respiration and fission at clinically relevant concentrations (e.g., 75 μM) [96]. Other beneficial effects of metformin reported are weight reduction [97], delay of aging [98,99], and reduced risk of COVID-19-related mortality [16,17]. In contrast, metformin use may cause adverse effects such as lactic acidosis, hepatotoxicity, acute pancreatitis, and vitamin B12 deficiency [100]. Due to these pleiotropic pharmacological and toxicological effects of metformin, this modeling analysis was pursued to gain improved understanding of its PK and tissue distribution properties among various species. Metformin PK were found in nine species owing to its wide use in the treatment of diabetes in clinical and veterinary settings for over 60 years. The PubMed search (last accessed 1 May 2021) provided 1733 citations since 1969 using the key words

'metformin' and 'pharmacokinetics' and 717 citations since 2010 with the topic of 'the pharmacokinetics of metformin'.

Metformin is well-known to be mostly or entirely eliminated via urinary excretion [40,73]. Though there has been some evidence of incomplete urinary recovery of metformin (e.g., approximately 80%) after IV doses in man [36,37] and rats [52,53,101], the systemic CL was comparable with RPF in most species, except for rabbits and cats (Figure 1). Since the glomerular filtration rate (essentially $f_{up} \cdot GFR$) is much smaller than RPF (Supplementary Table S2), the concordance between CL and RPF implies significant active secretion of metformin by the kidney. While hyperthermia (e.g., over 41 °C) is associated with decreased GFR and RPF [102], the RPF of relatively hyperthermic rabbits (39.1 °C) [103] was aligned with the fitted trendline between BW and RPF (Figure 1). This is consistent with the assessment that body temperature may be not a crucial term for allometric scaling across the mammalian species [104,105]. It is evident in the literature that renal transporters including organic cation transporters (OCT1 and OCT2) and multidrug and toxin extrusion proteins (MATE1 and MATE2) are involved in the active secretion of metformin [35]. Based on a quantitative proteomics approach, related transporters (e.g., OCT2 and MATE1) are highly expressed in the kidney, which were generally comparable among several species (e.g., mouse, rat, monkey, and man), arguing for the case that transporters are conserved [106]. While rabbits exhibited higher CL_R particularly for anionic drugs [45], which may be related to a higher extent of organic anion transporters (e.g., rbOAT1 and rbOAT3) compared to OCT transporters [107], discordant CL and RPF in rabbits (Figure 1) may be related to a lower affinity of metformin to rbOCT2 (e.g., IC50 value of 808 μM) than hOCT2 (339 μM) [108]. However, a previous PBPK model incorporating an electrogenic component for OCT1 and OCT2 transport suggested the plasma concentration profiles of metformin may be sensitive to transport activity mainly by MATE1/2 in the kidney [109,110]. Therefore, further studies to explain the systemic CL smaller than RPF in rabbit and cat with regard to the differential expression/activities in the apical membrane transport of metformin in their kidneys would be interesting.

As shown in Figure 3, the joint fitting of the mPBPK model reasonably captured the observed PK profiles for metformin in the nine species. One advantage of this approach is that fitting all profiles together allows the data to be shared in resolving the model parameters. The data from mice were rather limited, while most other species had more extensive measurements over longer times. Based on the in vitro PAMPA P of metformin (0.5×10^{-6} cm/s) [74], the apparent PAMPA P coefficient (i.e., $f_{up}P/R_b = 0.5 \times 10^{-6}$ cm/s) supported the finding of permeability-limited distribution in mPBPK modeling [79]. Another in vitro study [111] showed that PAMPA permeability increased from 0.15 to 0.75×10^{-6} cm/s with the increasing pH (i.e., pH ranging from 4.6 to 9.32), which indicates its low permeability over a range of physiologically relevant pH values. In addition to in vitro physicochemical properties, we alternatively applied a typical triexponential function for describing metformin PK (Supplementary Table S5). The total distributional clearance (CL_D) calculated from these in vivo observations [112,113] (i.e., with initial condition restricted to be $Dose/V_B$) was significantly lower than Q_{CO}, which also indicates that such modeling reveals that tissue permeability governs the rate of metformin distribution. It is noted that model-dependent CL values from the triexponential fitting were generally comparable with CL values from the separate fitting of mPBPK models in most species, except for dogs. This may be due to the overestimation of AUC in the triexponential function by restricting the initial condition to $Dose/V_B$ while the drug was an infused IV over 5 min (as we applied in the mPBPK models). Since f_{d1} (0.0390) is higher than f_{d2} (0.00677) (Table 2), Tissue 1 could be considered as rapidly perfused, while Tissue 2 as slowly perfused, when making a comparison to a traditional three-compartment model.

In this study, the apparent K_p values observed for tissues in mouse and rat were collected from the literature as listed in Table 6 (for detailed information, refer to Supplementary Table S3). The K_{p1} values for mouse (0.921) and rat (0.575) obtained from the separate fitting approach appeared to be somewhat underestimated considering the in vivo

tissue K_p values corresponding to Tissue 1 (e.g., for tissues other than muscle and skin, 0.213–11.3 in mouse and 0.956–4.63 in rat). Nevertheless, the K_{p2} values in the mPBPK modeling for mouse (1.44) and rat (0.466) were consistent with their muscle K_p (i.e., 1.03 for mouse and 0.597 for rat, averaged from multiple studies), supporting our kinetic assumption that Tissue 2 included muscle. For the larger species, however, the K_{p2} values were estimated to range from 0.675 to 7.53, which may imply species-dependent metformin partitioning to muscle and skin and/or different tissue components that are kinetically necessary for Tissue 2 in these species. Since metformin is a strong base (pKa = 11.8) and mainly exists in a cationic form in biological matrices, its binding to acidic phospholipids [114] and possible sequestration in the lysosomal/mitochondrial sub-compartments [115,116] may complicate its tissue distribution kinetics with regard to both the extent (K_p) and rate (f_d). Interestingly, the metformin distribution within cells showed that concentrations in the mitochondrial fraction (4.6 and 64.5 μM, after 22 h of metformin exposure in Hepa1-6 cells at 75 and 1000 μM) were significantly lower than in the cytosolic fraction (38.2 and 996 μM) [96].

OCT1 is expressed in the basolateral membrane of hepatocytes, which is a major site of pharmacological action for metformin inhibiting glucose production [117]. In the literature [118], the uptake rate of metformin into hepatocytes was highest in monkeys among four species (rats, monkeys, dogs, and man), which is consistent with the highest protein expression of hepatic OCT1 in monkeys [119]. These properties could contribute to the higher estimate of K_{p1} in monkeys (0.615) than rats (0.575) and man (0.484). Other distribution mechanisms may be involved, as V_{SS} is markedly higher in dogs (10.1 L/kg in Table 1 and 6.0 L/kg in Table 4). Similarly, the 4.4-fold higher metformin uptake by mOCT1 than by hOCT1, along with the comparable expression level of the transporter in the liver [120], was consistent with our K_{p1} values for mouse (0.921) and man (0.484). The higher uptake clearance normalized by the mRNA expression levels of hOCT1 compared to rOCT1 (with a factor of 13.1) [121] may explain the difference in our mPBPK model parameter f_{d1} between man (0.993) and rat (0.0694).

Based on the IV PK of metformin reasonably capturing the observations in nine species, the kinetic parameters for absorption could be estimated as shown in Figure 5. There was a decreasing bioavailability of metformin with increasing BW, which was associated with the decrease in its effective absorption rate constant $F \cdot k_a$. From a single-pass intestinal perfusion study in rats [33], $P_{eff,rat}$ was lower at a higher concentration of metformin (e.g., 47.1×10^{-6} at 10 μg/mL, and 27.0×10^{-6} cm/s at 200 μg/mL). The $P_{eff,rat}$ calculated from our mPBPK modeling (4.61×10^{-6} cm/s) was much lower than from this in situ study, probably because the 100 mg/kg oral dose given to rats may result in a luminal concentration of 4 mg/mL even under an assumption of instantaneous dissolution of the drug in the total fluid content of the stomach (2.29 g) and small intestine (3.89 g) [122]. This is much higher than 200 μg/mL, showing a probable saturable permeability. In addition, that a saturable oral absorption may be involved is also based on K_m values (1.15 to 4 mM) for uptake transporters in the apical membrane of human intestine (e.g., thiamine transporter 2 (THTR-2), plasma membrane monoamine transporter (PMAT), and serotonin reuptake transporter (SERT)) [35]. The differential apical uptake of metformin in the intestinal barrier between hTHTR-2 and mTHTR-2 transporters [123] may be related to the $P_{eff,man}$ (42.6×10^{-6} cm/s) being higher than $P_{eff,mouse}$ (7.0×10^{-6} cm/s). In addition, the decrease or knockout of OCT1 activity in man and mouse led to the increase of oral absorption of metformin [117]. Since mOCT1/hOCT1 transporters were suggested to play a crucial role in basolateral uptake of metformin into intestinal tissue [124], higher $P_{eff,man}$ may be involved with the species-dependent transport of metformin by intestinal OCT1. From our mPBPK modeling, the $P_{eff,in\ vivo}$ was estimated to be relatively higher in minipig, dog, and human than other species (Figure 5). Considering the probable absence of solubility limitations of metformin in gut lumen, species differences in $P_{eff,in\ vivo}$ may result, at least in part, from the water content per gut length being higher in pig, dog, and human [122], leading to enhanced active uptake across the gut wall with lower effective

concentrations in the lumen. The presence of THTR-2 and OCT1 transporters in the GI tract undoubtedly account for the high tissue-to-plasma ratios observed in mice and rats (Table 6).

Proctor et al. [34] examined metformin transport in Caco-2 cells to demonstrate carrier-mediated apical uptake that was seven-fold greater than basolateral efflux. The latter is limiting for transcellular transport and appears to account for the high metformin K_p values in GI tissues (Table 6). The $P_{eff,man}$ predicted from this in vitro Caco-2 permeability (e.g., $\log P_{eff} = 0.4926 \times \log P_{app} - 0.1454$, where $P_{app} = 500$ nm/s for metformin) [125] was 15.3 µm/s, which is comparable to $P_{eff,man}$ from our modeling analysis (42.6 µm/s). Based on the mPBPK model, metformin exhibits partial bioavailability in man ($F = 0.485$), compared to the fraction absorbed from the enteric compartment ($F_a = 0.185$) calculated from a physiological absorption model (e.g., $F_a = 1 - \left(1 + 0.54P_{eff}\right)^{-7}$, using the P_{eff} of 15.3 µm/s in the Advanced Compartmental Absorption and Transit (ACAT) model) [126]. Using T_{SI} and R (gut radius) values collected from the literature (Supplementary Table S2), the coefficient corresponding to P_{eff} term (i.e., $2T_{SI}/7R$) generally decreased with increasing body size. Thus, if there is no species difference in P_{eff}, which can be assumed to be the same with $P_{eff,rat}$ (e.g., 27.0×10^{-6} cm/s) or $P_{eff,man}$ predicted from Caco-2 cell permeability (e.g., 15.3×10^{-6} cm/s), the ACAT model consisting of seven enteric compartments argues for a decreasing F with increasing BW (Supplementary Figure S2). This assessment suggests that the joint role of metformin permeability and gut physiology accounts for the decreasing bioavailability with increasing BW in these species. Species differences in bioavailability were judged to be considerable for a variety of compounds in a literature review [127]. However, the general applicability of this conclusion for F_a needs further evaluation by factoring in the first-pass hepatic and gut wall extraction from the overall oral bioavailability.

Despite the abundant evidence for the involvement of carrier-mediated transport, the assumption of linear PK appeared to be adequate for describing the plasma PK of metformin in the current meta-analysis. In single-dose clinical studies [37,40], the terminal half-life of metformin based on urinary excretion rates was 4.22 to 5.11 times longer than that in plasma. However, this appears due to the longer sampling time in urine, which may better capture a late terminal phase. Metformin has a reported longer PK half-life when followed in erythrocytes (23.4 h) compared to plasma (2.7 h) after single doses [39]. This nonequilibrium between plasma and erythrocytes [37] is ascribed to a slow uptake ($t_{1/2} > 80$ h) and slow efflux ($t_{1/2} > 32$ h) from the cells [128]. While the PK profiles in these publications may not have been monitored over the same or for a sufficient period of time, Kajbaf et al. [129] followed metformin washout kinetics in patients with regard to both plasma and erythrocytes over 5 to 14 days. Although these patients had clinical complications, such as acute renal failure, the corresponding half-lives were 51.9 and 43.4 h. It is likely that many single-dose studies failed to assess metformin disposition over sufficiently long times to account for late phases and small amounts of the retained drug.

The marked difference between V_{SS} (6–10 L/kg for dogs and 0.432–0.856 L/kg for man) and $V_{d,area}$ (44.8 L/kg for dogs and 0.859–3.83 L/kg for man) [36,37,40,71] is likely related to differences in transporters and related tissue uptake. From the collected literature information (Supplementary Table S3), tissue K_p values at early times (e.g., <24 h) ranged 0.359 to 0.771 for muscle and 0.0354 for brain in mouse [55,130,131], while the prolonged treatment of metformin (i.e., from 7 to 30 days) produced K_p values of 1.00–2.06 for muscle and 0.174–0.257 for the brain [132]. Similarly in rats, the brain K_p increased from 0.2 (at 1 h) to 1.48 (at 24 h) [133], while the K_p values for muscle were 0.455 at 2 h of day 1 and 0.738 at 2 h of day 7 [134]. This time-dependent increase in tissue uptake of metformin may be related to differing terminal phase half-lives between the plasma and erythrocytes/tissues or may reflect drug-induced changes in the distribution. Collectively, therefore, carrier-mediated transport and/or continuous tissue redistribution may vary within or among species and alter the parameters in the PBPK model. More extensive studies that follow

plasma, tissue, and urinary excretion of metformin during multiple dosing and washout are needed.

An insightful assessment of metformin PK in dogs was carried out by Wesolowski et al. [71]. Their fitting algorithm accounts for the early distribution kinetics during and after the IV infusion (much like seen in PET scans by Gormsen et al. [135]) and handles the late disposition phase as a power function that captures the straight line phase on a log–log plot. This method applies a gamma-Pareto convolution that predicts slow continuing distribution consistent with the slow kinetics associated with red blood cells, the very low P-values (Table 5), and the small f_d values (Tables 2 and 4) for metformin. This approach yields a lower CL than the NCA analysis, and their mean CL was 15.1 compared to our mPBPK value of 19.3 mL/min/kg. It is also likely that V_{SS} values are underestimated when applying an exponential to a power function curve. While this elegant method may better capture the terminal phase of metformin PK in dogs, a species with unusually high V_{SS} (Table 1), it appears to be only applicable to single PK profiles and cannot, as yet, be utilized for tandem (oral and IV) PK profiles, as assessed here.

The present meta-assessment utilized the mPBPK modeling approach to compare the PK properties of metformin across nine species and supported the distribution model parameters with established calculation methods [81,82] in Table 5 and extensive tissue-to-plasma ratios for rodents summarized from the literature (Table 6). Typically, full PBPK models are built using both types of information. Burt et al. [109] utilized the Simcyp Simulator (Simcyp Ltd., Certara Co., Sheffield, UK) to predict metformin plasma concentrations in man, assuming $F = 0.7$, calculated K_p [114] values for various tissues, the k_a re-estimated using oral dose PK data, and renal and hepatic uptake related to transporter function with optimization using observed plasma and urinary excretion data. With such manipulations, single oral dose profiles of metformin were reasonably 'predicted'. Hanke et al. [42] carried out a similar PBPK modeling effort using PK-Sim® (Bayer Technology Services, Leverkusen, Germany) to capture the metformin profiles from 22 studies with doses ranging 0.001 to 2550 mg for up to 696 h during multiple dosing. The analysis included K_p values based on PET data obtained in plasma, blood, kidney, liver, intestines, and muscle over 1.5 h by Gormsen et al. [135]. Most of the assessment was based on matching plasma concentration profiles, which did not lend insight into longer time tissue distribution/accumulation kinetics of metformin.

The present meta-assessment has some limitations. While we sought all available PK studies of metformin that could be found in PubMed and by reference tracking, the drug has been subject to immense scrutiny, and undoubtedly, some relevant material may be missed. Diverse analytical methods ranging from early HPLC-UV to more recent LC-MS/MS may have a range of specificities and sensitivities (Table 1). Most of the data were digitized and dependent on published graphs with limitations based on single doses and in the duration of sampling (Figures 3 and 4). While metformin is purported to have linear kinetics (as we assumed), this depends on substrate exposures being lower than transporter K_m values. The washout PK in some species (like dogs) may better follow a power function, indicating complexities in distribution mechanisms that need tissue PK data and longer-term studies for better resolution. Nevertheless, the mPBPK models represent a state-of-the-art approach to modeling, summarizing, and comparing available single-dose profiles of metformin in the various species. Extending this modeling approach to include and compare oral and IV profiles across species provided unique insights into the absorption properties of metformin.

Upon completion of our analysis, Morse et al. [136] published a report demonstrating the interspecies comparison of the expression and activities of OCT transporters in the liver, which was investigated in relation to metformin PK. Using a single IV dose of 5-mg/kg metformin, wild-type rats showed comparable PK properties with the datasets (50, 100, and 200 mg/kg) used in the current analysis [52,53], in terms of CL (29.4 versus 23.6 to 26.4 mL/min/kg) and CL_R (i.e., 21.8 versus 17.8 to 19.5 mL/min/kg). Consistent with the previous PBPK model suggesting the importance of apical efflux process of metformin by

MATE1/2 transporters [109,110], single knockouts of the rOCT1 or rOCT2 transporters did not affect the plasma PK and tissue partitioning of metformin in rats. Different from man and mouse [117], however, knockout of the rOCT1 transporter exhibited no significant effect on the oral absorption of metformin in rats. It is noted that their measurements of metformin concentrations in plasma up to 24 h after IV administrations led to observing a longer half-life (5.12 h) compared to 2.1–2.5 h determined using the data for 10 h [52]. Thus, mean residence time in the body increased by using the longer half-life values resulted in higher V_{SS} (2.25 L/kg). The tissue-to-plasma ratios observed for various tissues at 4 h after the IV dose may govern the determination of $V_{d,area}$ rather than V_{SS} [137]. Tissue partitioning properties mostly in a range far above the V_{SS} value in the literature (2.25 L/kg) or in our current analysis (0.536 L/kg) may imply the involvement of low tissue permeability (Tables 2 and 4) and/or slow/continuous redistribution of metformin between plasma and tissues in rats, as discussed above.

In conclusion, we collected PK profiles from nine species for metformin, an effective antidiabetic agent widely used for various clinical and veterinary purposes. Utilizing a mPBPK model, the common features of metformin distribution that appear conserved among species were assessed in the joint fitting approach, while potential differences in PK parameters were evaluated in the individual fittings, with the results compared with the related literature data. Despite the lack of integrated information for tissue PK of metformin, a priori in silico calculations of physicochemical properties adopted in mPBPK models enabled the physiological interpretation of the absorption and disposition PK of metformin in various species. Unique perspectives were provided regarding the bioavailability that was found to be reduced with increased *BW*. This study provided a systematic review of the literature datasets and a quantitative analysis of metformin PK in all the available species and demonstrated the advantages of the simultaneous fitting of data from multiple species using system-specific physiological and anatomical variables. Further experimental studies are needed to resolve the mysteries of metformin absorption and distribution with the implementation of full and extended PBPK models utilizing longer term data to characterize its kinetics more completely.

4. Methods

4.1. Data Collection and Basic Allometric Scaling

The PK parameters for metformin including the systemic clearance (*CL*), oral clearance (*CL/F*), renal clearance (*CL_R*), and steady-state volume of distribution (V_{SS}) were collected from the literature for nine species (Table 1) based on a PubMed search and reference tracking. If not directly obtainable in the literature, these PK parameters were either calculated from available descriptors or obtained by noncompartmental analysis (NCA) of the plasma concentration–time profiles that were digitized from the published graphs using GetData Graph Digitizer version 2.26 (http://getdata-graph-digitizer.com/, accessed on 1 May 2021).

The physiological and anatomical variables necessary for mPBPK modeling were obtained for the species in which the metformin PK was found in the literature (mouse, rat, rabbit, cat, monkey, minipig, dog, man, and horse). The blood volumes were from one literature source [138], except for man [139]. The cardiac output for each species was determined by an allometric relationship [66]:

$$Q_{CO} = 0.235 \cdot BW^{0.75} \tag{1}$$

In addition, the renal plasma flow (*RPF*) [65–72], glomerular filtration rate (*GFR*) [70,105,140,141], gut radius (*R*) [70,142–146], luminal volume of the GI tract (V_{Lumen} for the stomach and small intestine) [122], and the small intestinal transit time (T_{SI}) [122,147–151] were obtained for each species. The detailed values including the anatomical volumes and blood perfusion rates to muscle (V_{MU}, Q_{MU}) and skin (V_{SK}, Q_{SK}) for the species-specific input variables are summarized in Supplementary Table S2. Allo-

metric relationships of these variables among the 9 species are provided in Supplementary Figure S1.

4.2. mPBPK Modeling via Joint Fittings

In the mPBPK model structure (Figure 2), blood and two peripheral tissue compartments (Tissues 1 and 2) were assumed. The differential equations used for the joint fitting are:

$$V_B R_b \frac{dC_p}{dt} = Input + Q_{CO} \cdot f_{d1} \cdot R_b \cdot \left(\frac{C_1}{K_p} - C_p \right) + Q_{CO} \cdot f_{d2} \cdot R_b \cdot \left(\frac{C_2}{K_p} - C_p \right) - CL \cdot C_p \quad (2)$$

$$V_1 \frac{dC_1}{dt} = Q_{CO} \cdot f_{d1} \cdot R_b \cdot \left(C_p - \frac{C_1}{K_p} \right) \quad (3)$$

$$V_2 \frac{dC_2}{dt} = Q_{CO} \cdot f_{d2} \cdot R_b \cdot \left(C_p - \frac{C_2}{K_p} \right) \quad (4)$$

where C_p is the plasma concentration of metformin, C_1 and C_2 are the metformin concentrations in Tissues 1 and 2, f_{d1} and f_{d2} are the fractional distribution parameters for Tissues 1 and 2, V_1 and V_2 are the anatomical volumes of Tissues 1 and 2, Q_{CO} is cardiac output, K_p is the tissue-to-plasma partition coefficient, R_b is the blood-to-plasma ratio, V_B is the blood volume, and CL is the systemic clearance. The IV *Input* was defined in accordance with the methodology of the literature source (e.g., bolus or short infusion, where $Input = \text{Dose}/\text{Duration of infusion}$). The initial conditions for C_1 and C_2 were set as zero. The blood partitioning properties of metformin (e.g., R_b and f_{up} (free fraction in the plasma)) were found to be in unity [39,109,128].

The *BW* (in kg) for each species was obtained from the publications with the metformin PK data (Table 1). The tissue volume fractions for Tissue 1 (f_t) and Tissue 2 ($1 - f_t$) were used to calculate V_1 and V_2, assuming the density of all tissues to be in unity:

$$V_1 = (BW - V_B) \cdot f_t \quad (5)$$

$$V_2 = (BW - V_B) \cdot (1 - f_t) \quad (6)$$

Due to the low permeability characteristics of metformin (e.g., in vitro PAMPA permeability of 0.5×10^{-6} cm/s) [74], the permeability-limited distribution [79] was assumed by using $f_{d,total}$ conserved across all species:

$$f_{d,total} = f_{d1} + f_{d2} \leq 1 \quad (7)$$

The primary estimated parameters, along with CL, were K_p, f_t, $f_{d,total}$, and f_{d1}, while f_{d2} was a secondary parameter. It can be noted that, except for CL, the other parameters are dimensionless.

4.3. mPBPK Modeling via Separate Fittings

Based on the collected PK data (Table 1), species differences were observed in metformin PK (e.g., bioavailability from 7.1% to 100% and V_{SS} from 0.321 to 10.1 L/kg). Since the involvement of various transporters is evident for metformin PK [35], there is a possibility that species-dependent transport activity may lead to different PK variables for each species. Therefore, we further conducted the mPBPK model fitting to oral and IV profiles for each species separately with the addition of more PK data.

A priori in silico calculation of the tissue distribution parameters (K_p) was carried out for 11 typical tissues of rats as applied in whole-body PBPK (WB-PBPK) models. Physicochemical (e.g., log P = −1.43, pKa = 11.8) [30,32] and blood partitioning properties of metformin ($f_{up} = 1$, $R_b = 1$) [39,109,128] were used. The K_p values from two calculation methods (i.e., Poulin and Theil [81], and Berezhkovskiy [82]) were applied for the prediction of V_{SS} amongst the four methods found in the GastroPlus PBPK simulator (version

9.8.0002; Simulations Plus, Inc., Lancaster, CA, USA). For the calculation of f_d, two approaches were considered for the tissue permeability coefficient P: (i) in vitro PAMPA P (0.5×10^{-6} cm/s) [74] and (ii) the P-value fitted to the rat PK data (0.0102×10^{-6} cm/s). For the latter case, a WB-PBPK model structure employing S_{eff} (i.e., the effective surface area across the interface between the systemic circulation and tissues) [79] was used. For the calculation of $f_{d,tissue}$:

$$f_{d,tissue} = 1 - e^{-\frac{fupS_{eff}P}{Q_T R_b}} \tag{8}$$

where Q_T is the blood flow to each tissue. Mean transit time (MTT) through the tissues was calculated as:

$$MTT = \frac{V_T K_p / R_b}{Q_T f_{d,tissue}} \tag{9}$$

where V_T is the anatomical tissue volume.

Compared to traditional compartment models, mPBPK models enable a more physiological interpretation of the systemic PK. Since f_t determined by the joint fitting was 0.172 with a single K_p assumption (see Results), it was reasoned that muscle, the anatomically largest organ, is included in Tissue 2 (e.g., $V_{MU}/(BW - V_B)$ ranges from 0.411 to 0.574 (>0.172) in the 9 species; Supplementary Table S2). Since our in silico calculations suggested skin as the kinetically largest tissue for variable P (see Results), then Tissue 2, the slowly equilibrating compartment, also included skin (i.e., calculated f_t value ranging from 0.472 to 0.678 for Tissue 2 in the 9 species). The differential equations used for the separate fittings are:

$$V_B R_b \frac{dC_p}{dt} = Input + Q_1 \cdot f_{d1} \cdot R_b \cdot \left(\frac{C_1}{K_{p1}} - C_p \right) + Q_2 \cdot f_{d2} \cdot R_b \cdot \left(\frac{C_2}{K_{p2}} - C_p \right) - CL \cdot C_p \tag{10}$$

$$V_1 \frac{dC_1}{dt} = Q_1 \cdot f_{d1} \cdot R_b \cdot \left(C_p - \frac{C_1}{K_{p1}} \right) \tag{11}$$

$$V_2 \frac{dC_2}{dt} = Q_2 \cdot f_{d2} \cdot R_b \cdot \left(C_p - \frac{C_2}{K_{p2}} \right) \tag{12}$$

where Q_2 is the blood flow rate to Tissue 2 ($Q_{MU} + Q_{SK}$), Q_1 is the blood flow rate to Tissue 1 ($Q_{CO} - Q_2$), V_2 is the anatomical volume of Tissue 2 ($V_{MU} + V_{SK}$), V_1 is the anatomical volume of Tissue 1 ($BW - V_B - V_2$), and K_{p1} and K_{p2} are the tissue-to-plasma partition coefficients for Tissues 1 and 2. The IV doses had bolus or infusion inputs, while, for the oral administration, the drug $Input$ from the absorption compartment is:

$$\frac{dX_a}{dt} = -k_a X_a \tag{13}$$

$$Input = F \cdot k_a \cdot X_a \tag{14}$$

where X_a is the drug amount at the absorption site with the initial condition of $X_a(0) = Dose$, k_a is the first-order absorption rate constant, and F is the bioavailability.

4.4. Model Fittings

For the nonlinear regression analysis, the maximum likelihood method in ADAPT 5 was used [152]. The variance model was:

$$V_i = (\sigma_1 + \sigma_2 Y_i)^2 \tag{15}$$

where V_i is the variance of the ith data point, Y_i is the ith model prediction, σ_1 and σ_2 are the variance model parameters that were estimated together with the system parameters during the model fittings. The goodness-of-fit of the model was monitored by visual inspection, Akaike Information Criterion (AIC), and Coefficient of Variation (CV%) of the

estimates. The ADAPT model code for the joint mPBPK is provided in the Supplementary Materials. The NCA were conducted using WinNonlin Professional 5.0.1. software (Pharsight Corporation, Mountain View, CA, USA).

Supplementary Materials: The following are available online at https://www.mdpi.com/article/10.3390/ph14060545/s1: Figure S1: Physiological and anatomical information (i.e., V_{SK}, V_{MU}, Q_{SK}, Q_{MU}, RPF, and GFR) collected from different sources (Supplementary Table S2) showed an allometric relationship among 9 species (i.e., mouse (0.025 kg), rat (0.25 kg), rabbit (2 kg), cat (5 kg), monkey (7 kg), minipig (14 kg), dog (28 kg), man (70 kg), and horse (530 kg))., Figure S2: ACAT model-based estimation of bioavailability using $F_a = 1 - \left(1 + 2P_{eff}T_{SI}/7R\right)^{-7}$ (7-enteric compartments), assuming that the effective intestinal permeability (P_{eff}) of the 9 species is the same with that of rat ($P_{eff,rat}$), and that of man ($P_{eff,man}$) predicted from Caco-2 cell permeability, which were compared with bioavailability determined from our mPBPK modeling (1-enteric compartment as a cylinder). Table S1: Literature reports and pharmacokinetic parameters of metformin given intravenously in different species. Table S2: Summary of the physiological input variables for the meta-analysis of metformin pharmacokinetics in various species. Table S3: Literature information collected for tissue distribution and blood partitioning of metformin. Table S4: Calculation of the steady-state volume of distribution (V_{SS}) using in vivo tissue K_p values based on the equation $V_{SS} = V_B + \sum V_{T,i}K_{p,i}$ [84]. Tissue K_p values were assumed to be muscle K_p (1.03 for mouse and 0.597 for rat) if unavailable in Table 6. Table S5: Model fitting results using a triexponential function ($C_p(t) = C_1 e^{-\lambda_1 t} + C_2 e^{-\lambda_2 t} + C_3 e^{-\lambda_3 t}$) for metformin PK in various species (CV% obtained by fitting). It is noted that five parameters (C_1, λ_1, C_2, λ_2, and λ_3) were optimized, while C_3 values were estimated as a secondary parameter ($C_3 = C_0 - C_1 - C_2$; $C_0 = Dose/V_B$). In addition, the ADAPT model code for the joint mPBPK is provided in the Supplementary Materials.

References

1. Hill, J. *The Vegetable System, or, the Internal Structure and the Life of Plants: Their Classes, Orders, Genera, and Species Ascertained and Described in a Method Altogether New: Comprehending an Artificial Index, and a Natural System: With Figures of all the Plants Designed and Engraved by the Author: The Whole from Nature Only*; Bradbury & Evans: London, UK, 1759; p. 54.
2. Bailey, C.J.; Day, C. Traditional Plant Medicines as Treatments for Diabetes. *Diabetes Care* **1989**, *12*, 553–564. [CrossRef]
3. Thomas, I.; Gregg, B. Metformin; a review of its history and future: From lilac to longevity. *Pediatr. Diabetes* **2017**, *18*, 10–16. [CrossRef]
4. Werner, E.A.; Bell, J. CCXIV—The preparation of methylguanidine, and of ββ-dimethylguanidine by the interaction of dicyanodiamide, and methylammonium and dimethylammonium chlorides respectively. *J. Chem. Soc. Trans.* **1922**, *121*, 1790–1794. [CrossRef]
5. Vecchio, I.; Tornali, C.; Bragazzi, N.L.; Martini, M. The Discovery of Insulin: An Important Milestone in the History of Medicine. *Front. Endocrinol.* **2018**, *9*, 613. [CrossRef] [PubMed]
6. Ungar, G.; Freedman, L.; Shapiro, S.L. Pharmacological Studies of a New Oral Hypoglycemic Drug. *Proc. Soc. Exp. Biol. Med.* **1957**, *95*, 190–192. [CrossRef] [PubMed]
7. Beringer, A. Zur Behandlung der Zuckerkrankheit mit Biguaniden. *Wien. Med. Wschr.* **1958**, *108*, 880–882.
8. Sterne, J. Du nouveau dans les antidiabetiques. La NN dimethylamine guanyl guanide (NNDG). *Maroc. Med.* **1957**, *36*, 1295–1296.

9. Pasik, C. *Diabetes and the Biguanides: The Mystery of Each*; Pasik, C., Ed.; Glucophage: Serving diabetology for 40 years; Groupe Lipha: Lyon, France, 1997; p. 79.

10. Nattrass, M.; Alberti, K. Biguanides. *Diabetologia* **1978**, *14*, 71–74. [CrossRef]

11. Nathan, D.M.; Buse, J.B.; Davidson, M.B.; Ferrannini, E.; Holman, R.R.; Sherwin, R.; Zinman, B. Medical Management of Hyperglycemia in Type 2 Diabetes: A Consensus Algorithm for the Initiation and Adjustment of Therapy: A consensus statement of the American Diabetes Association and the European Association for the Study of Diabetes. *Diabetes Care* **2008**, *32*, 193–203. [CrossRef]

12. United Kingdom Prospective Diabetes Study Group. Effect of intensive blood-glucose control with metformin on complications in overweight patients with type 2 diabetes (UKPDS 34). *Lancet* **1998**, *352*, 854–865. [CrossRef]

13. Evans, J.M.M.; Donnelly, L.A.; Emslie-Smith, A.M.; Alessi, D.R.; Morris, A.D. Metformin and reduced risk of cancer in diabetic patients. *BMJ* **2005**, *330*, 1304–1305. [CrossRef] [PubMed]

14. Li, D.; Yeung, S.C.J.; Hassan, M.M.; Konopleva, M.; Abbruzzese, J.L. Antidiabetic Therapies Affect Risk of Pancreatic Cancer. *Gastroenterology* **2009**, *137*, 482–488. [CrossRef]

15. Landman, G.W.; Kleefstra, N.; Van Hateren, K.J.; Groenier, K.H.; Gans, R.O.; Bilo, H.J. Metformin Associated with Lower Cancer Mortality in Type 2 Diabetes: ZODIAC-16. *Diabetes Care* **2009**, *33*, 322–326. [CrossRef] [PubMed]

16. Crouse, A.B.; Grimes, T.; Li, P.; Might, M.; Ovalle, F.; Shalev, A. Metformin Use Is Associated with Reduced Mortality in a Diverse Population With COVID-19 and Diabetes. *Front. Endocrinol.* **2021**, *11*, 600439. [CrossRef] [PubMed]

17. Bramante, C.T.; Ingraham, N.E.; Murray, T.A.; Marmor, S.; Hovertsen, S.; Gronski, J.; McNeil, C.; Feng, R.; Guzman, G.; Abdelwahab, N.; et al. Metformin and risk of mortality in patients hospitalised with COVID-19: A retrospective cohort analysis. *Lancet Health Longev.* **2021**, *2*, e34–e41. [CrossRef]

18. Bailey, C.J. Metformin: Historical overview. *Diabetologia* **2017**, *60*, 1566–1576. [CrossRef]

19. Le, S.; Lee, G.C. Emerging Trends in Metformin Prescribing in the United States from 2000 to 2015. *Clin. Drug Investig.* **2019**, *39*, 757–763. [CrossRef]

20. Miller, R.A.; Chu, Q.; Xie, J.; Foretz, M.; Viollet, B.; Birnbaum, M.J. Biguanides suppress hepatic glucagon signalling by decreasing production of cyclic AMP. *Nature* **2013**, *494*, 256–260. [CrossRef]

21. Madiraju, A.K.; Erion, D.M.; Rahimi, Y.; Zhang, X.-M.; Braddock, D.T.; Albright, R.A.; Prigaro, B.J.; Wood, J.L.; Bhanot, S.; Macdonald, M.J.; et al. Metformin suppresses gluconeogenesis by inhibiting mitochondrial glycerophosphate dehydrogenase. *Nature* **2014**, *510*, 542–546. [CrossRef] [PubMed]

22. Bailey, C.J.; Puah, J.A. Effect of metformin on glucose metabolism in mouse soleus muscle. *Diabete Metab.* **1986**, *12*, 212–218. [PubMed]

23. Rossetti, L.; De Fronzo, R.A.; Gherzi, R.; Stein, P.; Andraghetti, G.; Falzetti, G.; Shulman, G.I.; Klein-Robbenhaar, E.; Cordera, R. Effect of metformin treatment on insulin action in diabetic rats: In vivo and in vitro correlations. *Metab. Clin. Exp.* **1990**, *39*, 425–435. [CrossRef]

24. Kirpichnikov, D.; McFarlane, S.I.; Sowers, J.R. Metformin: An Update. *Ann. Intern. Med.* **2002**, *137*, 25–33. [CrossRef]

25. Bailey, C.J.; Mynett, K.J.; Page, T. Importance of the intestine as a site of metformin-stimulated glucose utilization. *Br. J. Pharmacol.* **1994**, *112*, 671–675. [CrossRef]

26. Ikeda, T.; Iwata, K.; Murakami, H. Inhibitory effect of metformin on intestinal glucose absorption in the perfused rat intestine. *Biochem. Pharmacol.* **2000**, *59*, 887–890. [CrossRef]

27. Stepensky, D.; Friedman, M.; Raz, I.; Hoffman, A. Pharmacokinetic-Pharmacodynamic Analysis of the Glucose-Lowering Effect of Metformin in Diabetic Rats Reveals First-Pass Pharmacodynamic Effect. *Drug Metab. Dispos.* **2002**, *30*, 861–868. [CrossRef]

28. Li, X.; Chen, Y.; Zhao, Z.; Lu, W.; Zhou, T. Pharmacokinetic/Pharmacodynamic Analysis of Metformin using Different Models in Diabetic Rats. *Drug Res.* **2016**, *66*, 547–554. [CrossRef] [PubMed]

29. Graham, G.G.; Punt, J.; Arora, M.; Day, R.O.; Doogue, M.; Duong, J.; Furlong, T.J.; Greenfield, J.R.; Greenup, L.C.; Kirkpatrick, C.M.; et al. Clinical Pharmacokinetics of Metformin. *Clin. Pharmacokinet.* **2011**, *50*, 81–98. [CrossRef]

30. Ray, P. Complex Compounds of Biguanides and Guanylureas with Metallic Elements. *Chem. Rev.* **1961**, *61*, 313–359. [CrossRef]

31. Cheng, C.-L.; Lawrence, X.Y.; Lee, H.-L.; Yang, C.-Y.; Lue, C.-S.; Chou, C.-H. Biowaiver extension potential to BCS Class III high solubility-low permeability drugs: Bridging evidence for metformin immediate-release tablet. *Eur. J. Pharm. Sci.* **2004**, *22*, 297–304. [CrossRef]

32. Schäfer, G.; Bojanowski, D. Interaction of Biguanides with Mitochondrial and Synthetic Membranes. *Eur. JBIC J. Biol. Inorg. Chem.* **1972**, *27*, 364–375. [CrossRef] [PubMed]

33. Song, N.-N.; Li, Q.-S.; Liu, C.-X. Intestinal permeability of metformin using single-pass intestinal perfusion in rats. *World J. Gastroenterol.* **2006**, *12*, 4064–4070. [CrossRef] [PubMed]

34. Proctor, W.R.; Bourdet, D.L.; Thakker, D.R. Mechanisms Underlying Saturable Intestinal Absorption of Metformin. *Drug Metab. Dispos.* **2008**, *36*, 1650–1658. [CrossRef]

35. Liang, X.; Giacomini, K.M. Transporters Involved in Metformin Pharmacokinetics and Treatment Response. *J. Pharm. Sci.* **2017**, *106*, 2245–2250. [CrossRef] [PubMed]

36. Sirtori, C.R.; Franceschini, G.; Galli-Kienle, M.; Cighetti, G.; Galli, G.; Bondioli, A.; Conti, F. Disposition of metformin (N, N-dimethylbiguanide) in man. *Clin. Pharmacol. Ther.* **1978**, *24*, 683–693. [CrossRef]

37. Tucker, G.T.; Casey, C.; Phillips, P.J.; Connor, H.; Ward, J.D.; Woods, H.F. Metformin kinetics in healthy subjects and in patients with diabetes mellitus. *Br. J. Clin. Pharmacol.* **1981**, *12*, 235–246. [CrossRef]

38. Sambol, N.C.; Chiang, J.; Lin, E.T.; Goodman, A.M.; Liu, C.Y.; Benet, L.Z.; Cogan, M.G. Kidney Function and Age Are Both Predictors of Pharmacokinetics of Metformin. *J. Clin. Pharmacol.* **1995**, *35*, 1094–1102. [CrossRef] [PubMed]

39. Robert, F.; Fendri, S.; Hary, L.; Lacroix, C.; Andréjak, M.; Lalau, J. Kinetics of plasma and erythrocyte metformin after acute administration in healthy subjects. *Diabetes Metab.* **2003**, *29*, 279–283. [CrossRef]

40. Pentikäinen, P.; Neuvonen, P.; Penttilä, A. Pharmacokinetics of metformin after intravenous and oral administration to man. *Eur. J. Clin. Pharmacol.* **1979**, *16*, 195–202. [CrossRef] [PubMed]

41. Wilcock, C.; Bailey, C.J. Accumulation of metformin by tissues of the normal and diabetic mouse. *Xenobiotica* **1994**, *24*, 49–57. [CrossRef]

42. Hanke, N.; Türk, D.; Selzer, D.; Ishiguro, N.; Ebner, T.; Wiebe, S.; Müller, F.; Stopfer, P.; Nock, V.; Lehr, T. A Comprehensive Whole-Body Physiologically Based Pharmacokinetic Drug–Drug–Gene Interaction Model of Metformin and Cimetidine in Healthy Adults and Renally Impaired Individuals. *Clin. Pharmacokinet.* **2020**, *59*, 1419–1431. [CrossRef]

43. Cao, Y.; Jusko, W.J. Applications of minimal physiologically-based pharmacokinetic models. *J. Pharmacokinet. Pharmacodyn.* **2012**, *39*, 711–723. [CrossRef]

44. Boxenbaum, H. Interspecies scaling, allometry, physiological time, and the ground plan of pharmacokinetics. *J. Pharmacokinet. Biopharm.* **1982**, *10*, 201–227. [CrossRef] [PubMed]

45. Jansen, K.; Casellas, C.P.; Groenink, L.; Wever, K.E.; Masereeuw, R. Humans are animals, but are animals human enough? A systematic review and meta-analysis on interspecies differences in renal drug clearance. *Drug Discov. Today* **2020**, *25*, 706–717. [CrossRef]

46. Hall, C.; Lueshen, E.; Mošat', A.; Linninger, A.A. Interspecies Scaling in Pharmacokinetics: A Novel Whole-Body Physiologically Based Modeling Framework to Discover Drug Biodistribution Mechanisms in vivo. *J. Pharm. Sci.* **2012**, *101*, 1221–1241. [CrossRef]

47. Song, D.; Jusko, W.J. Across-species meta-analysis of dexamethasone pharmacokinetics utilizing allometric and scaling modeling approaches. *Biopharm. Drug Dispos.* **2021**, *42*, 191–203. [CrossRef]

48. Zhao, J.; Cao, Y.; Jusko, W.J. Across-Species Scaling of Monoclonal Antibody Pharmacokinetics Using a Minimal PBPK Model. *Pharm. Res.* **2015**, *32*, 3269–3281. [CrossRef]

49. Huang, Q.; Gehring, R.; Tell, L.A.; Li, M.; Riviere, J.E. Interspecies allometric meta-analysis of the comparative pharmacokinetics of 85 drugs across veterinary and laboratory animal species. *J. Vet. Pharmacol. Ther.* **2015**, *38*, 214–226. [CrossRef]

50. Zhang, D. Evaluation of the Allometric Exponents in Prediction of Human Drug Clearance. Ph.D. Thesis, Virginia Commonwealth University, Richmond, VA, USA, 2014.

51. Johnston, C.A.; Dickinson, V.S.M.; Alcorn, J.; Gaunt, M.C. Pharmacokinetics and oral bioavailability of metformin hydrochloride in healthy mixed-breed dogs. *Am. J. Vet. Res.* **2017**, *78*, 1193–1199. [CrossRef] [PubMed]

52. Choi, Y.H.; Kim, S.G.; Lee, M.G. Dose-Independent Pharmacokinetics of Metformin in Rats: Hepatic and Gastrointestinal First-Pass Effects. *J. Pharm. Sci.* **2006**, *95*, 2543–2552. [CrossRef] [PubMed]

53. Choi, Y.; Lee, U.; Lee, B.; Lee, M. Pharmacokinetic interaction between itraconazole and metformin in rats: Competitive inhibition of metabolism of each drug by each other via hepatic and intestinal CYP3A1/2. *Br. J. Pharmacol.* **2010**, *161*, 815–829. [CrossRef]

54. Higgins, J.W.; Bedwell, D.W.; Zamek-Gliszczynski, M.J. Ablation of Both Organic Cation Transporter (Oct)1 and Oct2 Alters Metformin Pharmacokinetics but Has No Effect on Tissue Drug Exposure and Pharmacodynamics. *Drug Metab. Dispos.* **2012**, *40*, 1170–1177. [CrossRef] [PubMed]

55. Nakamichi, N.; Shima, H.; Asano, S.; Ishimoto, T.; Sugiura, T.; Matsubara, K.; Kusuhara, H.; Sugiyama, Y.; Sai, Y.; Miyamoto, K.-I.; et al. Involvement of Carnitine/Organic Cation Transporter OCTN1/SLC22A4 in Gastrointestinal Absorption of Metformin. *J. Pharm. Sci.* **2013**, *102*, 3407–3417. [CrossRef]

56. Bouriche, S.; Alonso-García, A.; Cárceles-Rodríguez, C.M.; Rezgui, F.; Fernández-Varón, E. Potential of sustained release microparticles of metformin in veterinary medicine: An in vivo pharmacokinetic study of metformin microparticles as oral sustained release formulation in rabbits. *BMC Vet. Res.* **2020**. [CrossRef]

57. Choi, J.S.; Choi, I. Drug interaction of metformin and aspirin in rabbits. *Korean J. Clin. Pharm.* **2003**, *13*, 67–71.

58. Michels, G.M.; Boudinot, F.D.; Ferguson, D.C.; Hoenig, M. Pharmacokinetics of the antihyperglycemic agent metformin in cats. *Am. J. Vet. Res.* **1999**, *60*, 738–742. [PubMed]

59. Nelson, R.; Spann, D.; Elliott, D.; Brondos, A.; Vulliet, R. Evaluation of the oral antihyperglycemic drug metformin in normal and diabetic cats. *J. Vet. Intern. Med.* **2004**, *18*, 18–24. [CrossRef] [PubMed]

60. Shen, H.; Liu, T.; Jiang, H.; Titsch, C.; Taylor, K.; Kandoussi, H.; Qiu, X.; Chen, C.; Sukrutharaj, S.; Kuit, K.; et al. Cynomolgus Monkey as a Clinically Relevant Model to Study Transport Involving Renal Organic Cation Transporters: In Vitro and In Vivo Evaluation. *Drug Metab. Dispos.* **2016**, *44*, 238–249. [CrossRef]

61. Heinig, K.; Bucheli, F. Fast liquid chromatographic-tandem mass spectrometric (LC–MS–MS) determination of metformin in plasma samples. *J. Pharm. Biomed. Anal.* **2004**, *34*, 1005–1011. [CrossRef] [PubMed]

62. Patel, N.J.; Yumibe, N.; Ruterbories, K.; Huang, N.; Burns, L.; Tan, J.; White, D.; Liu, J.; Brocksmith, D.; Bouchard, G.; et al. Pharmacokinetics of intravenous and oral metformin and r,s-verapamil in Sinclair, Hanford, Yucatan and Göttingen minipigs. *Int. J. Pharmacokinet.* **2017**, *2*, 81–91. [CrossRef]

63. Lee, S.H.; Kwon, K.-I. Pharmacokinetic-pharmacodynamic modeling for the relationship between glucose-lowering effect and plasma concentration of metformin in volunteers. *Arch. Pharm. Res.* **2004**, *27*, 806–810. [CrossRef] [PubMed]

64. Hustace, J.L.; Firshman, A.M.; Mata, J.E. Pharmacokinetics and bioavailability of metformin in horses. *Am. J. Vet. Res.* **2009**, *70*, 665–668. [CrossRef]

65. Thuesen, A.D.; Andersen, H.; Cardel, M.; Toft, A.; Walter, S.; Marcussen, N.; Jensen, B.L.; Bie, P.; Hansen, P.B.L. Differential effect of T-type voltage-gated Ca^{2+} channel disruption on renal plasma flow and glomerular filtration rate in vivo. *Am. J. Physiol. Renal Fluid Electrolyte Physiol.* **2014**, *307*, F445–F452. [CrossRef]

66. Brown, R.P.; Delp, M.D.; Lindstedt, S.L.; Rhomberg, L.R.; Beliles, R.P. Physiological Parameter Values for Physiologically Based Pharmacokinetic Models. *Toxicol. Ind. Health* **1997**, *13*, 407–484. [CrossRef] [PubMed]

67. Sweeney, L.M.; Kirman, C.R.; Gannon, S.A.; Thrall, K.D.; Gargas, M.L.; Kinzell, J.H. Development of a physiologically based pharmacokinetic (PBPK) model for methyl iodide in rats, rabbits, and humans. *Inhal. Toxicol.* **2009**, *21*, 552–582. [CrossRef] [PubMed]

68. Lindstedt, S.L.; Schaeffer, P.J. Use of allometry in predicting anatomical and physiological parameters of mammals. *Lab. Anim.* **2002**, *36*, 1–19. [CrossRef]

69. Jamei, M.; Marciniak, S.; Feng, K.; Barnett, A.; Tucker, G.; Rostami-Hodjegan, A. The Simcyp®Population-based ADME Simulator. *Expert Opin. Drug Metab. Toxicol.* **2009**, *5*, 211–223. [CrossRef] [PubMed]

70. Suenderhauf, C.; Parrott, N. A Physiologically Based Pharmacokinetic Model of the Minipig: Data Compilation and Model Implementation. *Pharm. Res.* **2012**, *30*, 1–15. [CrossRef]

71. Wesolowski, C.A.; Wanasundara, S.N.; Babyn, P.S.; Alcorn, J. Comparison of the gamma-Pareto convolution with conventional methods of characterising metformin pharmacokinetics in dogs. *J. Pharmacokinet. Pharmacodyn.* **2019**, *47*, 19–45. [CrossRef]

72. Holdstock, N.B.; Ousey, J.C.; Rossdale, P.D. Glomerular filtration rate, effective renal plasma flow, blood pressure and pulse rate in the equine neonate during the first 10 days post partum. *Equine Vet. J.* **1998**, *30*, 335–343. [CrossRef] [PubMed]

73. Beckmann, R. Absorption, distribution in the organism and elimination of metformin. *Diabetologia* **1969**, *5*, 318–324. [CrossRef]

74. Balimane, P.V.; Han, Y.-H.; Chong, S. Current industrial practices of assessing permeability and P-glycoprotein interaction. *AAPS J.* **2006**, *8*, E1–E13. [CrossRef]

75. Nestorov, I.A.; Aarons, L.J.; Arundel, P.A.; Rowland, M. Lumping of whole-body physiologically based pharmacokinetic models. *J. Pharmacokinet. Biopharm.* **1998**, *26*, 21–46. [CrossRef]

76. Björkman, S. Reduction and Lumping of Physiologically Based Pharmacokinetic Models: Prediction of the Disposition of Fentanyl and Pethidine in Humans by Successively Simplified Models. *J. Pharmacokinet. Pharmacodyn.* **2003**, *30*, 285–307. [CrossRef] [PubMed]

77. Gueorguieva, I.; Nestorov, I.A.; Rowland, M. Reducing Whole Body Physiologically Based Pharmacokinetic Models Using Global Sensitivity Analysis: Diazepam Case Study. *J. Pharmacokinet. Pharmacodyn.* **2006**, *33*, 1–27. [CrossRef]

78. Pilari, S.; Huisinga, W. Lumping of physiologically-based pharmacokinetic models and a mechanistic derivation of classical compartment models. *J. Pharmacokinet. Pharmacodyn.* **2010**, *37*, 365–405. [CrossRef] [PubMed]

79. Jeong, Y.-S.; Yim, C.-S.; Ryu, H.-M.; Noh, C.-K.; Song, Y.-K.; Chung, S.-J. Estimation of the minimum permeability coefficient in rats for perfusion-limited tissue distribution in whole-body physiologically-based pharmacokinetics. *Eur. J. Pharm. Biopharm.* **2017**, *115*, 1–17. [CrossRef]

80. Hemauer, S.J.; Patrikeeva, S.L.; Nanovskaya, T.N.; Hankins, G.D.; Ahmed, M.S. Role of human placental apical membrane transporters in the efflux of glyburide, rosiglitazone, and metformin. *Am. J. Obstet. Gynecol.* **2010**, *202*, 383.e1–383.e7. [CrossRef] [PubMed]

81. Poulin, P.; Theil, F. Prediction of Pharmacokinetics Prior to In Vivo Studies. 1. Mechanism-Based Prediction of Volume of Distribution. *J. Pharm. Sci.* **2002**, *91*, 129–156. [CrossRef]

82. Berezhkovskiy, L.M. Volume of Distribution at Steady State for a Linear Pharmacokinetic System with Peripheral Elimination. *J. Pharm. Sci.* **2004**, *93*, 1628–1640. [CrossRef] [PubMed]

83. Amidon, G.L.; Lennernäs, H.; Shah, V.P.; Crison, J.R. A theoretical basis for a biopharmaceutic drug classification: The correlation of in vitro drug product dissolution and in vivo bioavailability. *Pharm. Res.* **1995**, *12*, 413–420. [CrossRef] [PubMed]

84. Øie, S.; Tozer, T.N. Effect of Altered Plasma Protein Binding on Apparent Volume of Distribution. *J. Pharm. Sci.* **1979**, *68*, 1203–1205. [CrossRef]

85. Bailey, C.J.; Turner, R.C. Metformin. *N. Engl. J. Med.* **1996**, *334*, 574–579. [CrossRef]

86. De Fronzo, R.A. Pharmacologic Therapy for Type 2 Diabetes Mellitus. *Ann. Intern. Med.* **1999**, *131*, 281–303. [CrossRef] [PubMed]

87. Bailey, C.; Flatt, P.; Marks, V. Drugs inducing hypoglycemia. *Pharmacol. Ther.* **1989**, *42*, 361–384. [CrossRef]

88. Jeppesen, J.; Zhou, M.-Y.; Chen, Y.-D.I.; Reaven, G.M. Effect of Metformin on Postprandial Lipemia in Patients with Fairly to Poorly Controlled NIDDM. *Diabetes Care* **1994**, *17*, 1093–1099. [CrossRef]

89. De Fronzo, R.A.; Goodman, A.M. Efficacy of Metformin in Patients with Non-Insulin-Dependent Diabetes Mellitus. *N. Engl. J. Med.* **1995**, *333*, 541–549. [CrossRef]

90. De Fronzo, R.A.; Barzilai, N.; Simonson, D.C. Mechanism of Metformin Action in Obese and Lean Noninsulin-Dependent Diabetic Subjects. *J. Clin. Endocrinol. Metab.* **1991**, *73*, 1294–1301. [CrossRef]

91. Reaven, G.M.; Johnston, P.; Hollenbeck, C.B.; Skowronski, R.; Zhang, J.C.; Goldfine, I.D.; Chen, Y.D. Combined metformin-sulfonylurea treatment of patients with noninsulin-dependent diabetes in fair to poor glycemic control. *J. Clin. Endocrinol. Metab.* **1992**, *74*, 1020–1026. [CrossRef] [PubMed]

92. Lee, J.; Yesilkanal, A.E.; Wynne, J.P.; Frankenberger, C.; Liu, J.; Yan, J.; Elbaz, M.; Rabe, D.; Rustandy, F.D.; Tiwari, P.; et al. Effective breast cancer combination therapy targeting BACH1 and mitochondrial metabolism. *Nature* **2019**, *568*, 254–258. [CrossRef] [PubMed]

93. Saini, N.; Yang, X. Metformin as an anti-cancer agent: Actions and mechanisms targeting cancer stem cells. *Acta Biochim. Biophys. Sin.* **2017**, *50*, 133–143. [CrossRef]

94. Bridges, H.R.; Jones, A.J.Y.; Pollak, M.N.; Hirst, J. Effects of metformin and other biguanides on oxidative phosphorylation in mitochondria. *Biochem. J.* **2014**, *462*, 475–487. [CrossRef]

95. Dykens, J.A.; Jamieson, J.; Marroquin, L.; Nadanaciva, S.; Billis, P.A.; Will, Y. Biguanide-induced mitochondrial dysfunction yields increased lactate production and cytotoxicity of aerobically-poised HepG2 cells and human hepatocytes in vitro. *Toxicol. Appl. Pharmacol.* **2008**, *233*, 203–210. [CrossRef] [PubMed]

96. Wang, Y.; An, H.; Liu, T.; Qin, C.; Sesaki, H.; Guo, S.; Radovick, S.; Hussain, M.; Maheshwari, A.; Wondisford, F.E.; et al. Metformin Improves Mitochondrial Respiratory Activity through Activation of AMPK. *Cell Rep.* **2019**, *29*, 1511–1523.e1515. [CrossRef] [PubMed]

97. Malin, S.K.; Kashyap, S.R. Effects of metformin on weight loss: Potential mechanisms. *Curr. Opin. Endocrinol. Diabetes Obes.* **2014**, *21*, 323–329. [CrossRef] [PubMed]

98. Barzilai, N.; Crandall, J.P.; Kritchevsky, S.B.; Espeland, M.A. Metformin as a Tool to Target Aging. *Cell Metab.* **2016**, *23*, 1060–1065. [CrossRef]

99. Kulkarni, A.S.; Gubbi, S.; Barzilai, N. Benefits of Metformin in Attenuating the Hallmarks of Aging. *Cell Metab.* **2020**, *32*, 15–30. [CrossRef]

100. Shurrab, N.T.; Arafa, E.-S.A. Metformin: A review of its therapeutic efficacy and adverse effects. *Obes. Med.* **2020**, *17*, 100186. [CrossRef]

101. Choi, Y.H.; Lee, M.G. Effects of enzyme inducers and inhibitors on the pharmacokinetics of metformin in rats: Involvement of CYP2C11, 2D1 and 3A1/2 for the metabolism of metformin. *Br. J. Pharmacol.* **2006**, *149*, 424–430. [CrossRef]

102. Kanter, G.S. Glomerular filtration and renal plasma flow during hyperthermia. *Am. J. Physiol. Content* **1960**, *198*, 1044–1048. [CrossRef] [PubMed]

103. Boxenbaum, H.; Fertig, J.B. Scaling of antipyrine intrinsic clearance of unbound drug in 15 mammalian species. *Eur. J. Drug Metab. Pharmacokinet.* **1984**, *9*, 177–183. [CrossRef]

104. Yates, F.E.; Kugler, P.N. Similarity Principles and Intrinsic Geometries: Contrasting Approaches to Interspecies Scaling. *J. Pharm. Sci.* **1986**, *75*, 1019–1027. [CrossRef]

105. Lin, J.H. Species similarities and differences in pharmacokinetics. *Drug Metab. Dispos.* **1995**, *23*, 1008–1021.

106. Basit, A.; Radi, Z.; Vaidya, V.S.; Karasu, M.; Prasad, B. Kidney Cortical Transporter Expression across Species Using Quantitative Proteomics. *Drug Metab. Dispos.* **2019**, *47*, 802–808. [CrossRef] [PubMed]

107. Groves, C.E.; Suhre, W.B.; Cherrington, N.J.; Wright, S.H. Sex Differences in the mRNA, Protein, and Functional Expression of Organic Anion Transporter (Oat) 1, Oat3, and Organic Cation Transporter (Oct) 2 in Rabbit Renal Proximal Tubules. *J. Pharmacol. Exp. Ther.* **2005**, *316*, 743–752. [CrossRef]

108. Suhre, W.M.; Ekins, S.; Chang, C.; Swaan, P.W.; Wright, S.H. Molecular Determinants of Substrate/Inhibitor Binding to the Human and Rabbit Renal Organic Cation Transporters hOCT2 and rbOCT2. *Mol. Pharmacol.* **2005**, *67*, 1067–1077. [CrossRef] [PubMed]

109. Burt, H.; Neuhoff, S.; Almond, L.; Gaohua, L.; Harwood, M.; Jamei, M.; Rostami-Hodjegan, A.; Tucker, G.; Rowland-Yeo, K. Metformin and cimetidine: Physiologically based pharmacokinetic modelling to investigate transporter mediated drug–drug interactions. *Eur. J. Pharm. Sci.* **2016**, *88*, 70–82. [CrossRef] [PubMed]

110. Nishiyama, K.; Toshimoto, K.; Lee, W.; Ishiguro, N.; Bister, B.; Sugiyama, Y. Physiologically-Based Pharmacokinetic Modeling Analysis for Quantitative Prediction of Renal Transporter–Mediated Interactions between Metformin and Cimetidine. *CPT Pharmacomet. Syst. Pharmacol.* **2019**, *8*, 396–406. [CrossRef]

111. Yu, H.; Wang, Q.; Sun, Y.; Shen, M.; Li, H.; Duan, Y. A New PAMPA Model Proposed on the Basis of a Synthetic Phospholipid Membrane. *PLoS ONE* **2015**, *10*, e0116502. [CrossRef] [PubMed]

112. Veng-Pedersen, P. Theorems and implications of a model independent elimination/distribution function decomposition of linear and some nonlinear drug dispositions. I. Derivations and theoretical analysis. *J. Pharmacokinet. Biopharm.* **1984**, *12*, 627–648. [CrossRef]

113. Gillespie, W.R.; Veng-Pedersen, P. Theorems and implications of a model-independent elimination/distribution function decomposition of linear and some nonlinear drug dispositions. II. Clearance concepts applied to the evaluation of distribution kinetics. *J. Pharmacokinet. Biopharm.* **1985**, *13*, 441–451. [CrossRef]

114. Rodgers, T.; Leahy, D.; Rowland, M. Physiologically Based Pharmacokinetic Modeling 1: Predicting the Tissue Distribution of Moderate-to-Strong Bases. *J. Pharm. Sci.* **2005**, *94*, 1259–1276. [CrossRef]

115. Assmus, F.; Houston, J.B.; Galetin, A. Incorporation of lysosomal sequestration in the mechanistic model for prediction of tissue distribution of basic drugs. *Eur. J. Pharm. Sci.* **2017**, *109*, 419–430. [CrossRef] [PubMed]

116. Trapp, S.; Rosania, G.R.; Horobin, R.W.; Kornhuber, J. Quantitative modeling of selective lysosomal targeting for drug design. *Eur. Biophys. J.* **2008**, *37*, 1317–1328. [CrossRef] [PubMed]

117. Shu, Y.; Sheardown, S.A.; Brown, C.; Owen, R.P.; Zhang, S.; Castro, R.A.; Ianculescu, A.G.; Yue, L.; Lo, J.C.; Burchard, E.G.; et al. Effect of genetic variation in the organic cation transporter 1 (OCT1) on metformin action. *J. Clin. Investig.* **2007**, *117*, 1422–1431. [CrossRef] [PubMed]

118. Liao, M.; Zhu, Q.; Zhu, A.; Gemski, C.; Ma, B.; Guan, E.; Li, A.P.; Xiao, G.; Xia, C.Q. Comparison of uptake transporter functions in hepatocytes in different species to determine the optimal model for evaluating drug transporter activities in humans. *Xenobiotica* **2018**, *49*, 852–862. [CrossRef] [PubMed]

119. Wang, L.; Prasad, B.; Salphati, L.; Chu, X.; Gupta, A.; Hop, C.E.; Evers, R.; Unadkat, J.D. Interspecies Variability in Expression of Hepatobiliary Transporters across Human, Dog, Monkey, and Rat as Determined by Quantitative Proteomics. *Drug Metab. Dispos.* **2014**, *43*, 367–374. [CrossRef]

120. Meyer, M.J.; Tuerkova, A.; Römer, S.; Wenzel, C.; Seitz, T.; Gaedcke, J.; Oswald, S.; Brockmöller, J.; Zdrazil, B.; Tzvetkov, M.V. Differences in Metformin and Thiamine Uptake between Human and Mouse Organic Cation Transporter 1: Structural Determinants and Potential Consequences for Intrahepatic Concentrations. *Drug Metab. Dispos.* **2020**, *48*, 1380–1392. [CrossRef]

121. Kimura, N.; Masuda, S.; Tanihara, Y.; Ueo, H.; Okuda, M.; Katsura, T.; Inui, K.-I. Metformin is a Superior Substrate for Renal Organic Cation Transporter OCT2 rather than Hepatic OCT1. *Drug Metab. Pharmacokinet.* **2005**, *20*, 379–386. [CrossRef]

122. Hatton, G.B.; Yadav, V.; Basit, A.W.; Merchant, H.A. Animal Farm: Considerations in Animal Gastrointestinal Physiology and Relevance to Drug Delivery in Humans. *J. Pharm. Sci.* **2015**, *104*, 2747–2776. [CrossRef] [PubMed]

123. Liang, X.; Chien, H.-C.; Yee, S.W.; Giacomini, M.M.; Chen, E.C.; Piao, M.; Hao, J.; Twelves, J.; Lepist, E.-I.; Ray, A.S.; et al. Metformin Is a Substrate and Inhibitor of the Human Thiamine Transporter, THTR-2 (SLC19A3). *Mol. Pharm.* **2015**, *12*, 4301–4310. [CrossRef]

124. Wang, D.-S.; Jonker, J.W.; Kato, Y.; Kusuhara, H.; Schinkel, A.H.; Sugiyama, Y. Involvement of Organic Cation Transporter 1 in Hepatic and Intestinal Distribution of Metformin. *J. Pharmacol. Exp. Ther.* **2002**, *302*, 510–515. [CrossRef]

125. Gertz, M.; Harrison, A.; Houston, J.B.; Galetin, A. Prediction of Human Intestinal First-Pass Metabolism of 25 CYP3A Substrates from In Vitro Clearance and Permeability Data. *Drug Metab. Dispos.* **2010**, *38*, 1147–1158. [CrossRef]

126. Lawrence, X.Y.; Amidon, G.L. A compartmental absorption and transit model for estimating oral drug absorption. *Int. J. Pharm.* **1999**, *186*, 119–125.

127. Musther, H.; Olivares-Morales, A.; Hatley, O.J.; Liu, B.; Hodjegan, A.R. Animal versus human oral drug bioavailability: Do they correlate? *Eur. J. Pharm. Sci.* **2014**, *57*, 280–291. [CrossRef] [PubMed]

128. Xie, F.; Ke, A.B.; Bowers, G.D.; Zamek-Gliszczynski, M.J. Metformin's intrinsic blood-to-plasma partition ratio (B/P): Reconciling the perceived high in vivo B/P> 10 with the in vitro equilibrium value of unity. *J. Pharmacol. Exp. Ther.* **2015**, *354*, 225–229. [CrossRef]

129. Kajbaf, F.; Bennis, Y.; Hurtel-Lemaire, A.-S.; Andréjak, M.; Lalau, J.-D. Unexpectedly long half-life of metformin elimination in cases of metformin accumulation. *Diabet. Med.* **2015**, *33*, 105–110. [CrossRef] [PubMed]

130. Lee, N.; Duan, H.; Hebert, M.F.; Liang, C.J.; Rice, K.M.; Wang, J. Taste of a Pill. *J. Biol. Chem.* **2014**, *289*, 27055–27064. [CrossRef]

131. Toyama, K.; Yonezawa, A.; Masuda, S.; Osawa, R.; Hosokawa, M.; Fujimoto, S.; Inagaki, N.; Inui, K.; Katsura, T. Loss of multidrug and toxin extrusion 1 (MATE1) is associated with metformin-induced lactic acidosis. *Br. J. Pharmacol.* **2012**, *166*, 1183–1191. [CrossRef]

132. Chaudhari, K.; Wang, J.; Xu, Y.; Winters, A.; Wang, L.; Dong, X.; Cheng, E.Y.; Liu, R.; Yang, S.-H. Determination of metformin bio-distribution by LC-MS/MS in mice treated with a clinically relevant paradigm. *PLoS ONE* **2020**, *15*, e0234571. [CrossRef] [PubMed]

133. Łabuzek, K.; Suchy, D.; Gabryel, B.; Bielecka, A.; Liber, S.; Okopień, B. Quantification of metformin by the HPLC method in brain regions, cerebrospinal fluid and plasma of rats treated with lipopolysaccharide. *Pharmacol. Rep.* **2010**, *62*, 956–965. [CrossRef]

134. Ma, Y.-R.; Shi, A.-X.; Qin, H.-Y.; Zhang, T.; Wu, Y.-F.; Zhang, G.-Q.; Wu, X.-A. Metoprolol decreases the plasma exposure of metformin via the induction of liver, kidney and muscle uptake in rats. *Biopharm. Drug Dispos.* **2016**, *37*, 511–521. [CrossRef]

135. Gormsen, L.C.; Sundelin, E.I.; Jensen, J.B.; Vendelbo, M.H.; Jakobsen, S.; Munk, O.L.; Christensen, M.M.H.; Brøsen, K.; Frokiaer, J.; Jessen, N. In Vivo Imaging of Human 11C-Metformin in Peripheral Organs: Dosimetry, Biodistribution, and Kinetic Analyses. *J. Nucl. Med.* **2016**, *57*, 1920–1926. [CrossRef] [PubMed]

136. Morse, B.L.; Fallon, J.K.; Kolur, A.; Hogan, A.T.; Smith, P.C.; Hillgren, K.M. Comparison of Hepatic Transporter Tissue Expression in Rodents and Interspecies Hepatic OCT1 Activity. *AAPS J.* **2021**, *23*, 1–12. [CrossRef] [PubMed]

137. Berezhkovskiy, L.M. The Connection Between the Steady State (Vss) and Terminal (Vβ) Volumes of Distribution in Linear Pharmacokinetics and The General Proof That Vβ ≥ Vss. *J. Pharm. Sci.* **2007**, *96*, 1638–1652. [CrossRef] [PubMed]

138. Wolfensohn, S.; Lloyd, M. *Handbook of Laboratory Animal Management and Welfare*; John Wiley & Sons: Hoboken, NJ, USA, 2003.

139. Davies, B.; Morris, T. Physiological Parameters in Laboratory Animals and Humans. *Pharm. Res.* **1993**, *10*, 1093–1095. [CrossRef] [PubMed]

140. Von Hendy-Willson, V.E.; Pressler, B.M. An overview of glomerular filtration rate testing in dogs and cats. *Vet. J.* **2011**, *188*, 156–165. [CrossRef] [PubMed]

141. Walsh, D.; Royal, H. Evaluation of a single injection of 99mTc-labeled diethylenetriaminepentaacetic acid for measuring glomerular filtration rate in horses. *Am. J. Vet. Res.* **1992**, *53*, 776–780.

142. Kararli, T.T. Comparison of the gastrointestinal anatomy, physiology, and biochemistry of humans and commonly used laboratory animals. *Biopharm. Drug Dispos.* **1995**, *16*, 351–380. [CrossRef] [PubMed]

143. Ferraris, R.P.; Lee, P.P.; Diamond, J.M. Origin of regional and species differences in intestinal glucose uptake. *Am. J. Physiol. Gastrointest. Liver Physiol.* **1989**, *257*, 689. [CrossRef]

144. Merchant, H.A.; McConnell, E.L.; Liu, F.; Ramaswamy, C.; Kulkarni, R.P.; Basit, A.W.; Murdan, S. Assessment of gastrointestinal pH, fluid and lymphoid tissue in the guinea pig, rabbit and pig, and implications for their use in drug development. *Eur. J. Pharm. Sci.* **2011**, *42*, 3–10. [CrossRef]

145. Bettini, G.; Muracchini, M.; Della Salda, L.; Preziosi, R.; Morini, M.; Guglielmini, C.; Sanguinetti, V.; Marcato, P. Hypertrophy of intestinal smooth muscle in cats. *Res. Vet. Sci.* **2003**, *75*, 43–53. [CrossRef]

146. Clauss, M.; Frey, R.; Kiefer, B.; Lechner-Doll, M.; Loehlein, W.; Polster, C.; Streich, W.J. The maximum attainable body size of herbivorous mammals: Morphophysiological constraints on foregut, and adaptations of hindgut fermenters. *Oecologia* **2003**, *136*, 14–27. [CrossRef]

147. Myagmarjalbuu, B.; Moon, M.J.; Heo, S.H.; Jeong, S.I.; Park, J.-S.; Jun, J.Y.; Jeong, Y.Y.; Kang, H.K. Establishment of a Protocol for Determining Gastrointestinal Transit Time in Mice Using Barium and Radiopaque Markers. *Korean J. Radiol.* **2013**, *14*, 45–50. [CrossRef] [PubMed]

148. Quini, C.C.; Américo, M.F.; Corá, L.A.; Calabresi, M.F.; Alvarez, M.; Oliveira, R.B.; A Miranda, J.R. Employment of a noninvasive magnetic method for evaluation of gastrointestinal transit in rats. *J. Biol. Eng.* **2012**, *6*, 6. [CrossRef] [PubMed]

149. Davies, R.R.; Davies, J.A.R. Rabbit gastrointestinal physiology. *Vet. Clin. N. Am. Exot. Anim. Pract.* **2003**, *6*, 139–153. [CrossRef]

150. Chandler, M.L.; Guilford, G.; Lawoko, C.R. Radiopaque Markers to Evaluate Gastric Emptying and Small Intestinal Transit Time in Healthy Cats. *J. Vet. Intern. Med.* **1997**, *11*, 361–364. [CrossRef] [PubMed]

151. Steinmann, M.; Bezugley, R.J.; Bond, S.L.; Pomrantz, J.S.; Léguillette, R. A wireless endoscopy capsule suitable for imaging of the equine stomach and small intestine. *J. Vet. Intern. Med.* **2020**, *34*, 1622–1630. [CrossRef] [PubMed]

152. D'Argenio, D.Z.; Schumitzky, A.; Wang, X. *ADAPT 5 User's Guide: Pharmacokinetic/Pharmacodynamic Systems Analysis Software*; Biomedical Simulations Resource: Los Angeles, CA, USA, 2009.